Diversity in Weakly Coordinating Anions. Mono- and Polynuclear Halo(perfluoroaryl)metalates as Cocatalysts for Stereospecific Olefin Polymerization: Synthesis, Structure, and Reactivity

Ming-Chou Chen, John A. S. Roberts, Afif M. Seyam, Liting Li, Cristiano Zuccaccia, Nicholas G. Stahl, and Tobin J. Marks*

Department of Chemistry, Northwestern University, Evanston, Illinois 60208-3113

Received September 27, 2005

A series of mononuclear and polynuclear trityl (perfluoroaryl)borate, -aluminate, and -gallate reagents, potential cocatalysts/activators for metallocene-mediated olefin polymerization, have been synthesized via fluoride abstraction from trityl fluoride (Ph_3CF) by the organo Lewis acid reagents $B(C_6F_5)_3$ (**1**), $B(o\text{-}C_6F_5C_6F_4)_3$ (**2**), and $Al(C_6F_5)_3$ (**3**), by derivatization of $Ph_3C^+FAl(o\text{-}C_6F_5C_6F_4)_3^-$ (**4**), and by reaction of trityl fluoride with in situ generated $Ga(C_6F_5)_3$ (**5**). Reaction of trityl fluoride with the tris(perfluoroaryl)-boranes **1** and **2** yields the trityl tris(perfluoroaryl)fluoroborates $Ph_3C^+FB(C_6F_5)_3^-$ (**6**) and $Ph_3C^+FB(o\text{-}C_6F_5C_6F_4)_3^-$ (**7**), respectively. The three trityl tris(perfluorophenyl)fluoroaluminates $(Ph_3C^+)_xF_x[Al(C_6F_5)_3]_y^{x-}$ ($x = 1$, $y = 1$, **8**; $x = 1$, $y = 2$, **9**; $x = 2$, $y = 3$, **10**) can be isolated from the reaction of trityl fluoride with the tris(perfluoroaryl)alane **3** in the appropriate molar ratios. Reaction of the trityl tris(perfluoroaryl)-fluoroaluminate **4** with **3** affords the asymmetric fluoro-bridged trityl bis[tris(perfluoroaryl)]aluminate $Ph_3C^+(C_6F_5)_3AlFAl(o\text{-}C_6F_5C_6F_4)_3^-$ (**11**), while reaction of the trityl halides Ph_3CCl and Ph_3CBr with **3** gives the corresponding trityl tris(perfluorophenyl)haloaluminates $Ph_3C^+XAl(C_6F_5)_3^-$ (X = Cl, **12**; X = Br, **13**). The isolable, symmetric fluoro-bridged trityl bis[tris(perfluoroaryl)]gallate $Ph_3C^+F[Ga(C_6F_5)_3]_2^-$ (**14**) is derived from a "one-pot" reaction of trityl fluoride with $Ga(C_6F_5)_3$, generated in situ from **4** + $Ga(CH_3)_3$. Of these new species, compounds **7** and **10**−**14** were characterized by single-crystal X-ray diffraction. Trityl salts **6**−**13** react with the C_s-symmetric metallocene precatalyst $Me_2C(Cp)(Flu)ZrMe_2$ (**15**: Cp = C_5H_4; Flu = $C_{13}H_8$, fluorenyl) to form isolable ion-pair complexes or characterizable mixtures. Species **6** reacts with **15** to generate the known ion pair $Me_2C(Cp)(Flu)ZrMe^+MeB(C_6F_5)_3^-$ (**16**), and reaction of **7** with **15** gives the fluoro-bridged dimeric diastereomers $[Me_2C(Cp)(Flu)ZrMe]_2(\mu\text{-}F)^+FB(o\text{-}C_6F_5C_6F_4)_3^-$ (**17**). The trityl tris(perfluorophenyl)fluoroaluminates **8**−**10** all react with **15** to afford mixtures of $Me_2C(Cp)(Flu)ZrMe^+FAl(C_6F_5)_3^-$ (**18**) and diastereomeric $[Me_2C(Cp)(Flu)ZrMe]_2(\mu\text{-}Me)^+(C_6F_5)_3AlFAl(C_6F_5)_3^-$ (**19**). Asymmetric species **11** cleanly affords the diastereomeric $[Me_2C(Cp)(Flu)ZrMe]_2(\mu\text{-}Me)^+(C_6F_5)_3AlFAl(o\text{-}C_6F_5C_6F_4)_3^-$ (**20**) in reaction with the metallocene **15**. Adducts of **12** and **13** with the metallocene **15** afford the decomposition products $Me_2C(Cp)(Flu)ZrCl(C_6F_5)$ (**21**) and $[Me_2C(Cp)(Flu)Zr(\mu_2\text{-}Br)]_2^{2+}[Al(C_6F_5)_4^-]_2$ (**22**), respectively. Complexes **17**−**22** were characterized by single-crystal X-ray diffraction.

Introduction

Recent developments in understanding cation−anion interactions in metallocenium/single-site ion-pair polymerization catalyst systems (**A**, produced via reaction of neutral metallocenes with neutral or ionic organometalloid activators; eq 1) reveal

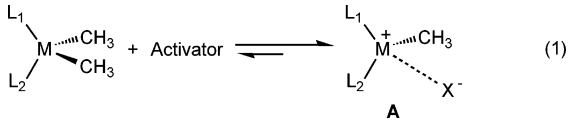

(1)

that the nature of the cation−anion interaction has a profound influence on catalyst lifetime and stability, polymerization activity, chain-transfer pathways, and stereoregulation.[1,2] Well-known activator/cocatalyst classes include alkylaluminoxanes (e.g. MAO and MMAO),[3] tris(perfluorophenyl)borane ($B(C_6F_5)_3$; **1**)[4] and related perfluoroarylboranes,[5] ammonium or trityl salts of $B(C_6F_5)_4^-$ [6] and related perfluoroarylborates,[7] perfluoroaryl-alanes (e.g. $Al(C_6F_5)_3$; **7**),[8] and (perfluoroaryl)fluoroaluminate salts.[9] Systems with single-molecule activators exhibiting clean activation chemistry and affording characterizable active catalysts (e.g., with $B(C_6F_5)_3$ and Ph_3C^+ $B(C_6F_5)_4^-$)[1,4,6] allow correlation of catalyst ion-pair structural and dynamic features with polymerization behavior. These catalyst systems exhibit varying modes of cation−anion interaction and are found to be 1:1 contact ion pairs at typical polymerization concentrations in low-ϵ media.[10,11]

In general, the product polymer M_w value, polydispersity, and (with prochiral propylene as monomer) the relative abundances of various stereosequences in the polymer backbone are sensitive to counteranion identity in a systematic way.[12] For C_s-symmetric precatalysts, these observables reflect the rate of propylene insertion *relative to* the rates of competing stereodefect generation and chain termination processes, according to the estab-

(1) For recent reviews, see: (a) Gibson, V. C.; Spitzmesser, S. K. *Chem. Rev.* **2003**, *103*, 283−315. (b) Pédeutour, J.-N.; Radhakrishnan, K.; Cramail, H.; Deffieux, A. *Macromol. Rapid Commun.* **2001**, *22*, 1095−1123. (c) Chen, Y.-X.; Marks, T. J. *Chem. Rev.* **2000**, *100*, 1391−1434. (d) Gladysz, J. A., Ed. *Chem. Rev.* **2000**, *100*, 1167−1682. (e) *Topics in Catalysis*; Marks, T. J., Stevens, J. C., Eds.; Kluwer: Dordrecht, The Netherlands, 1999; Vol. 7, pp 1−208. (f) Britovsek, G. J. P.; Gibson, V. C.; Wass, D. F. *Angew. Chem., Int. Ed.* **1999**, *38*, 428−447.

10.1021/om0508334 CCC: $33.50
Publication on Web 04/19/2006

lished mechanism for syndiospecific propylene enchainment.[13] The strength and nature of the ion pairing is found to play a key role in determining the *absolute* rates of these individual processes. These systematic correlations, explored in detail in recently published work,[12] are briefly summarized here. In isolated ion-pair complexes formed by reaction of the C_s-symmetric metallocene **15** with a collection of cocatalyst reagents/activators of the present class, the cation−anion contact is apparently dictated by the structure of the anion and exhibits a diverse variety of motifs.

Complex **15** + **1**, for example, exhibits a largely electrostatic cation−anion interaction,[14] with the $MeB(C_6F_5)_3^-$ anionic

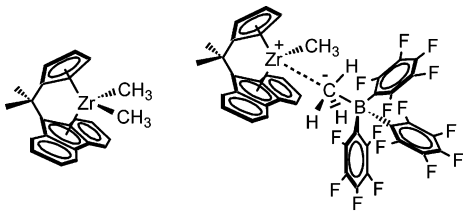

15 **15 + 1 (16)**

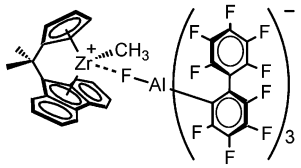

15 + 4

fragment bound at the available coordination site of the cationic Zr center, the anion methide group acting as a bridge between the Zr and B atoms. This cation−anion interaction is observed by NMR to be rather labile, and monomer insertion proceeds rapidly in polymerization experiments with this catalyst system.[12] However, for the catalyst derived from **15** + **4**, the anion is coordinated via the Al-bound fluorine atom, this interaction being significantly more inert. Insertion is dramatically attenuated, as are (to a greater degree) chain termination and stereodefect-forming reorganization processes. In stark contrast to these results, with **15** + $Ph_3C^+B(C_6F_5)_4^-$ (irreversibly and quantitatively releasing Ph_3CCH_3), the highly symmetric, charge-dispersed $B(C_6F_5)_4^-$ anion binds rather loosely with no obviously dominant preferred interatomic contact, and all polymerization-related processes proceed much more rapidly, particularly propylene enchainment.[12] As with $B(C_6F_5)_4^-$, the anions in catalyst systems **15** + **2** and **15** + B(perfluoronaphthyl)$_3$ appear to be more weakly bound to the cationic fragment than is the anion generated by reaction of precatalyst **15** with **1**, on the basis of polymerization reactivity data. Room-temperature polymerization data do not alone provide direct evidence that these specific cation−anion interactions persist during catalytic turnover. However, the observed systematic dependence of the absolute rates of observed polymerization-related processes on anion identity and the nature of the cation−anion interaction in the isolated catalyst ion pairs inferred from crystallographic and solution-phase dynamic NMR analysis suggest that this is likely the case. Indeed, early observations of anion effects in polymerization experiments stimulated efforts to develop new single-

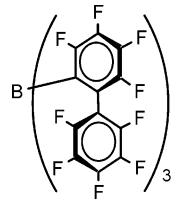

2

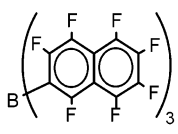

B(perfluoronaphthyl)$_3$

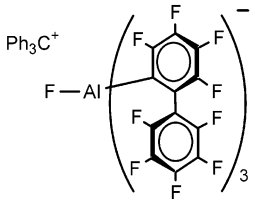

4

(2) For recent cocatalyst studies, see: (a) Busico, V.; Cipullo, R.; Cutillo, F.; Vacatello, M.; Castelli, V. V. *Macromolecules* **2003**, *36*, 4258−4261. (b) Mohammed, M.; Nele, M.; Al-Humydi, A.; Xin, S.; Stapleton, R. A.; Collins, S. *J. Am. Chem. Soc.* **2003**, *125*, 7930−7941. (c) Abramo, G. P.; Li, L.; Marks, T. J. *J. Am. Chem. Soc.* **2002**, *124*, 13966−13967. (d) Li, L.; Metz, M. V.; Li, H.; Chen, M.-C.; Marks, T. J. *J. Am. Chem. Soc.* **2002**, *124*, 12725−12741. (e) Metz, M. V.; Schwartz, D. J.; Stern, C. L.; Marks, T. J.; Nickias, P. N. *Organometallics* **2002**, *21*, 4159−4168. (f) Metz, M. V.; Sun, Y. M.; Stern, C. L.; Marks, T. J. *Organometallics* **2002**, *21*, 3691−3702. (g) Wilmes, G. M.; Polse, J. L.; Waymouth, R. M. *Macromolecules* **2002**, *35*, 6766−6772. (h) Lancaster, S. J.; Rodriguez, A.; Lara-Sanchez, A.; Hannant, M. D.; Walker, D. A.; Hughes, D. H.; Bochmann, M. *Organometallics* **2002**, *21*, 451−453. (i) Rodriguez, G.; Brant, P. *Organometallics* **2001**, *20*, 2417−2420. (j) Kaul, F. A. R.; Puchta, G. T.; Schneider, H.; Grosche, M.; Mihalios, D.; Herrmann, W. A. *J. Organomet. Chem.* **2001**, *621*, 177−183. (k) Chen, Y.-X.; Kruper, W. J.; Roof, G.; Wilson, D. R. *J. Am. Chem. Soc.* **2001**, *123*, 745−746. (l) Zhou, J.; Lancaster, S. J.; Walker, D. A.; Beck, S.; Thornton-Pett, M.; Bochmann, M. *J. Am. Chem. Soc.* **2001**, *123*, 223−237. (m) Kehr, G.; Roesmann, R.; Frohlich, R.; Holst, C.; Erker, G. *Eur. J. Inorg. Chem.* **2001**, 535−538. (n) Mager, M.; Becke, S.; Windisch, H.; Denninger, U. *Angew. Chem., Int. Ed.* **2001**, *40*, 1898−1902.

(3) (a) Sinn, H.; Kaminsky, W. *Adv. Organomet. Chem.* **1980**, *18*, 99−149. (b) Sinn, H.; Kaminsky, W.; Vollmer, H.-J.; Woldt, R. *Angew. Chem., Int. Ed. Engl.* **1980**, *19*, 390−392.

(4) (a) Yang, X.; Stern, C. L.; Marks, T. J. *J. Am. Chem. Soc.* **1994**, *116*, 10015−10031. (b) Yang, X.; Stern, C. L.; Marks, T. J. *J. Am. Chem. Soc.* **1991**, *113*, 3623−3625.

(5) (a) Li, L.; Stern, C. L.; Marks, T. J. *Organometallics* **2000**, *19*, 3332−3337. (b) Li, L.; Marks, T. J. *Organometallics* **1998**, *17*, 3996−4003. (c) Chen, Y.-X.; Stern, C. L.; Yang, S.; Marks, T. J. *J. Am. Chem. Soc.* **1996**, *118*, 12451−12452. (d) See also refs 2c−e. (e) For a recent chelating borane review, see: Piers, W. E.; Irvine, G. J.; Williams, V. C. *Eur. J. Inorg. Chem.* **2000**, 2131−2142.

(6) (a) Chien, J. C. W.; Tsai, W.-M.; Rausch, M. D. *J. Am. Chem. Soc.* **1991**, *113*, 8570−8571. (b) Yang, X.; Stern, C. L.; Marks, T. J. *Organometallics* **1991**, *10*, 840−842. (c) Ewen, J. A.; Elder, M. J. Eur. Pat. Appl. 426637, 1991; *Chem. Abstr.* **1991**, *115*, 136987c, 136988d.

(7) For related fluorinated tetraarylborates, see the following: (a) References 2h−j,l. (b) Jia, L.; Yang, X.; Stern, C. L.; Marks, T. J. *Organometallics* **1997**, *16*, 842−857. (c) Jia, L.; Yang, X.; Ishihara, A.; Marks, T. J. *Organometallics* **1995**, *14*, 3135−3137.

(8) (a) Reference 2f. (b) Bochmann, M.; Sarsfield, M. J. *Organometallics* **1998**, *17*, 5908−5912. (c) Biagini, P.; Lugli, G.; Abis, L.; Andreussi, P. U.S. Patent 5,602,269, 1997.

(9) (a) Chen, Y.-X.; Metz, M. V.; Li, L.; Stern, C. L.; Marks, T. J. *J. Am. Chem. Soc.* **1998**, *120*, 6287−6305. (b) Chen, Y.-X.; Stern, C. L.; Marks, T. J. *J. Am. Chem. Soc.* **1997**, *119*, 2582−2583. (c) Elder, M. J.; Ewen, J. A. Eur. Pat. Appl. EP 573,403, 1993; *Chem. Abstr.* **1994**, *121*, 0207d.

(10) (a) Stahl, N. G.; Zuccaccia, C.; Jensen, T. R.; Marks, T. J. *J. Am. Chem. Soc.* **2003**, *125*, 5256−5257. (b) Stahl, N. G.; Marks, T. J.; Macchioni, A.; Zuccaccia, C. Presented in part at the 222nd National Meeting of the American Chemical Society, Chicago, IL, August 2001, abstract INOR 407. (c) Zuccaccia, C.; Stahl, N. G.; Macchioni, A.; Chen, M.-C.; Roberts, J. A. S.; Marks, T. J. *J. Am. Chem. Soc.* **2004**, *126*, 1448−1464.

(11) Song, F.; Lancaster, S. J.; Cannon, R. D.; Schormann, M.; Humphrey, S. M.; Zuccaccia, C.; Macchioni, A.; Bochmann, M. *Organometallics* **2005**, *24*, 1315.

(12) Chen, M.-C.; Roberts, J. A. S.; Marks, T. J. *J. Am. Chem. Soc.* **2004**, *126*, 4605−4625.

(13) (a) Resconi, L.; Cavallo, L.; Fait, A.; Piemontesi, F. *Chem. Rev.* **2000**, *100*, 1253−1345. (b) Coates, G. W. *Chem. Rev.* **2000**, *100*, 1223−1252. (c) Veghini, D.; Henling, L. M.; Burkhardt, T. J.; Bercaw, J. E. *J. Am. Chem. Soc.* **1999**, *121*, 564−573. (d) Ewen, J. A.; Jones, R. L.; Razavi, A.; Ferrara, J. D. *J. Am. Chem. Soc.* **1988**, *110*, 6255−6256.

molecule cocatalysts, leading to the development of the sterically encumbered perfluoroaryl group 13 cocatalysts B(*o*-$C_6F_5C_6F_4)_3$ (**2**),[5c] B(perfluoronaphthyl)$_3$,[5b] and the trityl tris(perfluoroaryl)-fluoroaluminate salt $Ph_3C^+FAl(o\text{-}C_6F_5C_6F_4)_3^-$ (**4**).[9a] This research represents a facet of the important continuing search for weakly coordinating anionic species.[15] The catalyst systems afforded by these new cocatalysts and their antecedents exhibit a broad range of thermal stabilities, with the more active systems being in general less stable. These collected observations have therefore motivated and directed the development of single-site catalyst systems that are both highly active and more thermally robust.

Recently we communicated several new classes of mononuclear and polynuclear fluoro(perfluoroaryl)borate, -aluminate, and -gallate cocatalysts.[16] These more sterically encumbered and charge-dispersing cocatalysts afford thermally stable active catalyst systems that can produce highly stereoregular polypropylenes with very high polymerization activities.[17] In the present report, we extend our preliminary findings,[16] discuss the syntheses of new and previously reported species in detail, and describe observed spectroscopic, structural, and reactivity trends of these new cocatalysts. We also discuss the chemistry of these new cocatalysts as activators for the metallocene precatalyst **15** as well as the spectroscopic and structural properties of ion-pair complexes produced in these activation reactions. In a complementary account[17] we compare/contrast the propylene polymerization behavior of the active catalyst systems derived from this new series of cocatalysts in combination with the archetypal C_s-symmetric precatalyst **15** and with the C_1-symmetric precatalyst Me_2Si(CpR*)(octahydrofluorenyl)-$ZrMe_2$ (R* = (1*R*,2*S*,5*R*)-*trans*-5-methyl-*cis*-2-(2-propyl)cyclohexyl, (−)-menthyl). In certain interesting and instructive cases, we observe high stereoselectivities in conjunction with high polymerization activities with both of these precatalysts.[17]

Experimental Section

Materials and Methods. All manipulations of air-sensitive materials were performed with rigorous exclusion of oxygen and moisture in flamed Schlenk-type glassware on a dual-manifold Schlenk line or interfaced to a high-vacuum line (10^{-6} Torr) or in an N_2-filled Vacuum Atmospheres or MBraun glovebox with a high-capacity recirculator (<1 ppm of O_2). Argon (Matheson, prepurified) was purified by passage through a supported MnO-packed oxygen removal column and a column packed with activated Davidson 4A molecular sieves. Hydrocarbon solvents (toluene and pentane) were distilled under nitrogen from Na/benzophenone ketyl or passed through columns packed with molecular sieves and supported Cu(0) deoxygenating agent. These solvents were subsequently stored under vacuum over Na/K alloy in Teflon-valved bulbs and distilled using a high-vacuum line immediately prior to use. Deuterated solvents were obtained from Cambridge Isotope Laboratories (all ≥99 atom % D), freeze−pump−thaw degassed, dried over Na/K alloy, and stored in resealable flasks. Other nonhalogenated solvents were dried over Na/K alloy, and halogenated solvents were distilled from CaH_2. Trityl fluoride (Ph_3CF),[18] $B(C_6F_5)_3$ (**1**),[19] B(*o*-$C_6F_5C_6F_4)_3$ (**2**),[5c] $Al(C_6F_5)_3\cdot0.5C_7H_8$ (**3**),[20] $Ph_3C^+FAl(o\text{-}C_6F_5C_6F_4)_3^-$ (**4**),[9a] and Me_2C(Cp)(Flu)$ZrMe_2$ (**15**)[21] were prepared according to literature procedures. Trityl bromide and trityl chloride (Aldrich, 98%) were used as received. The reagents $Ph_3C^+FB(C_6F_5)_3^-$ (**6**), $Ph_3C^+FB(o\text{-}C_6F_5C_6F_4)_3^-$ (**7**), $Ph_3C^+FAl(C_6F_5)_3^-$ (**8**), $Ph_3C^+F[Al(C_6F_5)_3]_2^-$ (**9**), $(Ph_3C^+)_2F_2[Al(C_6F_5)_3]_3^{2-}$ (**10**), $Ph_3C^+(C_6F_5)_3AlFAl(o\text{-}C_6F_5C_6F_4)_3^-$ (**11**), and $Ph_3C^+F[Ga(C_6F_5)_3]_2^-$ (**14**) were prepared as described in the Supporting Information accompanying ref 16.

Physical and Analytical Measurements. NMR spectra were recorded on Varian UNITY Inova-500 (FT: 500 MHz, ^{1}H; 125 MHz, ^{13}C), UNITY Inova-400 (FT: 400 MHz, ^{1}H; 100 MHz, ^{13}C), and Mercury-400 (FT: 400 MHz, ^{1}H; 100 MHz, ^{13}C; 377 MHz, ^{19}F) instruments. Chemical shifts for ^{1}H and ^{13}C spectra were referenced using internal solvent resonances and are reported relative to tetramethylsilane. ^{19}F NMR spectra were referenced to external $CFCl_3$. NMR experiments on air-sensitive samples were conducted in Teflon-valve-sealed NMR tubes (J. Young).

Synthesis of $Ph_3C^+ClAl(C_6F_5)_3^-$ (12). In the glovebox, Ph_3CCl (70 mg, 0.25 mmol), $Al(C_6F_5)_3\cdot0.5C_7H_8$ (**3**; 114 mg, 0.200 mmol),[20] and 5 mL of toluene were loaded into a 50 mL reaction flask having a filter frit, and then the flask was reattached to the vacuum line. The mixture was stirred for 1.0 h at room temperature, and 20 mL of pentane was next condensed into the flask. The resulting suspension was filtered, and the collected orange solid was washed three times with 10 mL of pentane. This recrystallization procedure from toluene/pentane was repeated until the pure title compound was obtained; yield 133 mg, 83%. ^{1}H NMR (C_7D_8, 23 °C): δ 6.8−7.4 (br, Ph). ^{19}F NMR (C_7D_8, 23 °C): δ −122.354 (m, 6 F, *o*-F), −156.706 (m, 3 F, *p*-F), −163.79 (m, 6 F, *m*-F). Anal. Calcd for $C_{37}H_{15}AlClF_{15}$: C, 55.07; H, 1.87. Found: C, 54.72; H, 2.12. Orange crystals of the title complex suitable for X-ray diffraction were obtained by slow diffusion of pentane into toluene solutions. With a 1:2 ratio of Ph_3CCl and $Al(C_6F_5)_3\cdot0.5C_7H_8$, three new ^{19}F resonances are observed. ^{19}F NMR (C_7D_8, 23 °C): −123.015 (m, 6 F, *o*-F), −154.960 (m, 3 F, *p*-F), −163.705 (m, 6 F, *m*-F). However, crystals suitable for X-ray diffraction grown by slow diffusion of pentane into toluene solutions of the reaction mixture were of a polymorph of previously characterized crystalline **12**.

Synthesis of $Ph_3C^+BrAl(C_6F_5)_3^-$ (13). In a procedure similar to that described above but using Ph_3CBr (80 mg, 0.25 mmol) in place of Ph_3CCl, the title compound was obtained; yield 121 mg, 71%. ^{1}H NMR (C_7D_8, 23 °C): δ 6.8−7.4 (br, Ph). ^{19}F NMR (C_7D_8, 23 °C): δ −122.44 (m, 6 F, *o*-F), −156.85 (m, 3 F, *p*-F), −163.73 (m, 6 F, *m*-F). Anal. Calcd for $C_{37}H_{15}AlBrF_{15}$: C, 52.20; H, 1.78. Found: C, 52.05; H, 2.01. Orange crystals of the title complex suitable for X-ray diffraction were obtained by slow diffusion of pentane into toluene solutions. Similar to the previous reaction, with a 1:2 ratio of Ph_3CBr and $Al(C_6F_5)_3\cdot0.5C_7H_8$, three new ^{19}F resonances were observed. Crystals suitable for X-ray diffraction, isolated by slow diffusion of pentane into toluene solutions of this reaction mixture, were found to be **13**.

General Procedure for Reaction of Me_2C(Cp)(Flu)$ZrMe_2$ (15) with Cocatalysts Studied by in Situ NMR. In a typical procedure,

(14) (a) Lanza, G.; Fragala, I. L.; Marks, T. J. *Organometallics* **2002**, *21*, 5594−5612. (b) Lanza, G.; Fragala, I. L.; Marks, T. J. *Organometallics* **2001**, *20*, 4006−4017. (c) Lanza, G.; Fragala, I. L.; Marks, T. J. *J. Am. Chem. Soc.* **2000**, *122*, 12764−12777.

(15) (a) Juhasz, M.; Hoffmann, S.; Stoyanov, E.; Kim, K.-C.; Reed, C. A. *Angew. Chem., Int. Ed.* **2004**, *43*, 5352−5355. (b) Reed, C. A. *Acc. Chem. Res.* **1998**, *31*, 133−139. (c) Seppelt, K. *Angew. Chem., Int. Ed.* **1993**, *32*, 1025−1027.

(16) Preliminary communication: Chen, M.-C.; Roberts, J. A. S.; Marks, T. J. *Organometallics* **2004**, *23*, 932−935.

(17) Polymerization results using the present series of cocatalysts with metallocenes **15** and Me_2Si(CpR*)(octahydrofluorenyl)$ZrMe_2$ (**2**, R* = (1*R*,2*S*,5*R*)-*trans*-5-methyl-*cis*-2-(2-propyl)cyclohexyl; (−)-menthyl) will be published elsewhere (Roberts, J. A. S.; Chen, M.-C. C.; Marks, T. J. Manuscript in preparation).

(18) Oishi, M.; Yamamoto, H. *Bull. Chem. Soc. Jpn.* **2001**, *74*, 1445−1454.

(19) Massey, A. G.; Park, A. J. *J. Organomet. Chem.* **1964**, *2*, 245−250.

(20) This compound was prepared as a toluene adduct.[8b,c] *Caution!* $Al(C_6F_5)_3$ has been reported to detonate on attempted sublimation at elevated temperatures. Pohlmann, J. L. W.; Brinckmann, F. E. *Z. Naturforsch., B* **1965**, *20B*, 5. Chambers, R. D. *Organomet. Chem. Rev.* **1966**, *1*, 279.

(21) (a) Razavi, A.; Thewalt, U. *J. Organomet. Chem.* **1993**, *445*, 111−114. (b) Razavi, A.; Ferrara, J. *J. Organomet. Chem.* **1992**, *435*, 299−310.

in the glovebox, $Me_2C(Cp)(Flu)ZrMe_2$ (**15**) and the required cocatalyst in a 1:1 stoichiometric ratio were loaded into a J. Young NMR tube, and 0.5 mL of toluene-d_8 was transferred in. Each sample was then shaken vigorously and transferred directly to the NMR spectrometer probe. In all cases, complete consumption of complex **1** was observed by ^1H and ^{19}F NMR, along with the formation of Ph_3CCH_3 and the corresponding ion-pair complex.

Experimental descriptions and chemical shift data for the in situ NMR study of $Me_2C(Cp)(Flu)ZrMe_2$ (**15**) activation by $Ph_3C^+FB(C_6F_5)_3^-$ (**6**), $Ph_3C^+FB(o\text{-}C_6F_5C_6F_4)_3^-$ (**7**), $Ph_3C^+FAl(C_6F_5)_3^-$ (**8**), $Ph_3C^+F[Al(C_6F_5)_3]_2^-$ (**9**), $(Ph_3C^+)_2F_2[Al(C_6F_5)_3]_3^{2-}$ (**10**), and $Ph_3C^+(C_6F_5)_3AlFAl(o\text{-}C_6F_5C_6F_4)_3^-$ (**11**) are presented in the Supporting Information accompanying ref 16.

In Situ NMR Study of $Me_2C(Cp)(Flu)ZrMe_2$ (15) Activation by $Ph_3C^+ClAl(C_6F_5)_3^-$ (12) or $Ph_3C^+BrAl(C_6F_5)_3^-$ (13). $Me_2C(Cp)(Flu)ZrMe_2$ (**15**; 3.9 mg, 0.010 mmol) and one of the above cocatalysts were loaded into two NMR tubes, as described in the above procedure. Rapid methide abstraction from **15** by both of these cocatalysts to form Ph_3CCH_3 was observed, and multiple products were detected in the three reaction mixtures. However, due to overlap of the fluorenyl signals in the ^1H NMR, complete and unambiguous identification of the derived species was not possible. Nevertheless, orange crystals of $Me_2C(Cp)(Flu)ZrCl(C_6F_5)$ (**21**, from reaction of **15** + **12**) and doubly bridged $[Me_2C(Cp)(Flu)Zr(\mu\text{-}Br)]_2^{2+}[Al(C_6F_5)_4^-]_2$ (**22**, from reaction of **15** + **13**) suitable for X-ray diffraction were obtained by slow diffusion of pentane into toluene solutions of the above reaction mixtures at 0 °C.

X-ray Crystal Structure Determinations of $Ph_3C^+ClAl(C_6F_5)_3^-$ (12), $Ph_3C^+BrAl(C_6F_5)_3^-$ (13), $[Me_2C(Cp)(Flu)ZrMe]_2(\mu\text{-}F)^+FB(o\text{-}C_6F_5C_6F_4)_3^-$ (17), $[Me_2C(Cp)(Flu)ZrMe]_2(\mu\text{-}Me)^+F[Al(C_6F_5)_3]_2^-$ (19), $[Me_2C(Cp)(Flu)ZrMe]_2(\mu\text{-}Me)^+[(C_6F_5)_3AlFAl(2\text{-}C_6F_5C_6F_4)_3]^-$ (20), $Me_2C(Cp)(Flu)ZrCl(C_6F_5)$ (21), and $[Me_2C(Cp)(Flu)Zr(\mu\text{-}Br)]_2^{2+}[Al(C_6F_5)_4^-]_2$ (22). Crystals of the title complexes suitable for X-ray diffraction were obtained as described above by slow diffusion of pentane into toluene solutions, either at room temperature or at 0 °C. Inside the glovebox, the crystals were placed on a glass slide and covered with dry Infineum V8512 oil. The crystals were then removed from the box, and a suitable crystal was chosen under a microscope using plane-polarized light. The crystal was mounted on a glass fiber and transferred to a Bruker SMART 1000 CCD area detector diffractometer in a nitrogen cold stream at 153(2) K. Twenty frames (20 s exposures, 0.3° slices) were collected in three areas of space to determine the orientation matrix. The parameters for data collection were determined by the peak intensities and widths from the 60 frames used to determine the orientation matrix. The faces of the crystal were then indexed and data collection was begun. After data collection, the frames were integrated, the initial crystal structure was solved by direct methods, the structure solution was expanded through successive least-squares cycles, absorption corrections were applied, and the final solution was determined. Crystal data, data collection, and refinement parameters are summarized in Table 1. Data for the previously reported structures $Ph_3C^+FB(o\text{-}C_6F_5C_6F_4)_3^-$ (**7**), $(Ph_3C^+)_2F_2[Al(C_6F_5)_3]_3^{2-}$ (**10**), $Ph_3C^+(C_6F_5)_3AlFAl(o\text{-}C_6F_5C_6F_4)_3^-$ (**11**), and $Ph_3C^+F[Ga(C_6F_5)_3]_2^-$ (**14**) have been reprocessed to ensure consistency with the newly reported structures.

Results and Discussion

In the following sections, we discuss the syntheses, solid-state structures, and solution structural/dynamic features of the (perfluoroaryl)metalate complexes **6**−**14**, their reaction chemistry with $Me_2C(Cp)(Flu)ZrMe_2$ (**15**), and the products generated in these reactions.

The discussion is presented in five parts: in the first we provide an overview of the syntheses and general features of new cocatalysts **6**−**14**; in the second, we briefly survey the activation chemistry of group 4 metallocene dimethyl precatalysts with the single-molecule cocatalyst/anion precursors and give an overview of activation reactions between cocatalysts **6**−**14** with precatalyst **15**; the third, fourth, and fifth sections are devoted to B-, Al- and Ga-containing species, respectively: in each, we detail the syntheses, spectroscopic, and structural features of the coctalysts and then describe the activation chemistry of these cocatalyst species with metallocene **15** and the spectroscopic and structural features of the resultant metallocenium ion-pair complexes. The collected spectroscopic, structural, and reactivity data are examined independently and as parts of the whole, to provide a complete picture of these interesting and complex systems.

I. Synthesis and Characterization of Cocatalysts 6−14. General Considerations. The species presented herein constitute a new class of sterically encumbered, highly charge delocalized (perfluoroaryl)metalate cocatalyst/counteranions, offering a variety of substituents with differing coordinative tendencies, classified according to the general synthetic route by which they are accessed: under oxygen- and moisture-free conditions, trityl halides are combined with known neutral and ionic perfluoroaryl complexes of boron, aluminum, and gallium in varying stoichiometries to yield trityl salt species featuring metalloid−halogen linkages. Specific isolable mono- and polymetallic trityl(perfluoroaryl)metal halide salts are accessible in this way and in some cases exhibit remarkable performance as cocatalysts in propylene polymerization with the zirconocene dialkyls $Me_2C(Cp)(Flu)ZrMe_2$ (**15**) and $Me_2Si(Cp\text{-}(-)\text{-menthyl})(octahydrofluorenyl)ZrMe_2$; these polymerization results and their mechanistic implications are presented in detail elsewhere.[17]

The common structural theme across this series of cocatalysts is the presence of one or more metalloid-bound halogen atoms found in either M−X or M−X−M bonding configurations; the synthetic and metallocene activation chemistry typically involves formation or cleavage of these metalloid−halogen bonds. The group 13 atoms of these species also bear strongly electron-withdrawing perfluoroaryl substituents that impart considerably heightened Lewis acidity to the corresponding neutral tris(perfluoroaryl)metalloid analogues and are thought to play a key role in anion charge delocalization, in addition to providing steric bulk. In the present series, these substituents are either simple perfluorophenyl (C_6F_5) groups or *o*-perfluorobiphenyl ($o\text{-}C_6F_5C_6F_4$) groups, the latter capable of sterically encapsulating *or* exposing the metalloid-bound halogen or C atoms, depending on the steric context of these potentially bridging moieties (vide infra).

The new cocatalysts described below have been isolated and characterized by standard 1-D $^1H/^{19}F$ NMR and analytical techniques (see the Experimental Section for details). Scheme 1 illustrates the general synthetic route by which cocatalyst reagents **6**−**10** and **14** are obtained. Of these, six have been further characterized by single-crystal X-ray diffraction. Comparison of the structures of cocatalysts **4**, **7**, and **10**−**14** (Table 2) reveals, not surprisingly, that (a) the M−X bond distances increase with increasing summed ionic radii: B−F < Ga−(μ-F) < Al−Cl < Al−Br, (b) the M−C_{aryl} bond distances increase with increasing metalloid covalent radius, as B−C_{aryl} < Al−C_{aryl} ≈ Ga−C_{aryl}, and (c) the unassociated Ph_3C^+ cations are virtually identical in all cocatalyst crystal structures. The breadth of available species and combined ^{19}F NMR, solid-state

Table 1. Summary of Crystal Structure Data for Cocatalysts 7 and 10−14 and Complexes 17, 19, and 20−22[a]

	7	10	11	12	13	14	17	19	20	21	22
formula	$C_{57.5}H_{18}BF_{28}$	$C_{105}H_{30}Al_3F_{47}$	$C_{83.5}H_{19}Al_2F_{43}$	$C_{37}H_{15}AlClF_{15}$	$C_{37}H_{15}AlBrF_{15}$	$C_{55}H_{15}Ga_2F_{31}$	$C_{94}H_{58}BF_{29}Zr_2$	$C_{43.25}H_{16.5}AlF_{15.5}Zr$	$C_{111}H_{50}Al_2F_{43}Zr_2$	$C_{54}H_{36}Cl_2F_{10}Zr_2$	$C_{48.5}H_{18}AlBrF_{20}Zr$
formula wt	1251.53	2265.23	1892.95	806.92	851.38	1404.11	1931.65	948.76	2436.91	1128.17	1178.74
cryst color, habit	yellow, needle	orange, plate	yellow, plate	yellow, block	yellow, plate	yellow, needle	red, block	red, plate	red, needle	red, needle	green/yellow, plate
cryst dimens (mm)	0.454 × 0.104 × 0.070	0.442 × 0.158 × 0.128	0.310 × 0.200 × 0.066	0.248 × 0.142 × 0.104	0.488 × 0.104 × 0.074	0.508 × 0.104 × 0.084	0.280 × 0.124 × 0.094	0.438 × 0.252 × 0.026	0.382 × 0.080 × 0.036	0.324 × 0.044 × 0.038	0.868 × 0.300 × 0.024
cryst syst	triclinic	triclinic	triclinic	monoclinic	monoclinic	monoclinic	triclinic	monoclinic	triclinic	monoclinic	triclinic
space group	$P\bar{1}$	$P\bar{1}$	$P\bar{1}$	$P2_1/c$	$P2_1/c$	$P2_1/c$	$P\bar{1}$	$C2/c$	$P\bar{1}$	$P2_1/c$	$P\bar{1}$
a, Å	9.718(3)	12.6562(11)	13.3346(13)	12.3098(8)	12.510(9)	15.975(2)	16.0202(16)	11.9646(8)	12.947(2)	8.7197(15)	14.145(4)
b, Å	14.501(4)	13.2621(12)	14.3315(14)	7.8476(5)	7.896(5)	14.134(2)	16.9357(17)	21.1165(14)	17.518(3)	15.908(3)	14.570(4)
c, Å	18.768(5)	30.7946(27)	21.134(2)	33.702(2)	33.79(2)	23.140(3)	17.3241(17)	30.680(2)	23.134(4)	15.612(3)	15.542(4)
α, deg	85.523(4)	85.8182(15)	90.371(2)	90	90	90	112.792(2)	90	84.617(3)	90	111.423(5)
β, deg	82.419(4)	87.6169(16)	104.966(2)	97.732(10)	97.512(14)	101.368(2)	106.482(2)	101.237(1)	79.768(3)	91.030(3)	100.320(5)
γ, deg	74.328(4)	76.1506(15)	94.913(2)	90	90	90	101.012(2)	90	84.966(3)	90	112.691(5)
V, Å^3	2521.8(11)	5003.6(13)	3885.7(7)	3226.1(4)	3309(4)	5122.5(12)	3907.0(7)	7602.8(9)	5127.1(17)	2165.3(6)	2552.9(13)
Z	2	2	2	4	4	4	2	8	2	4	2
d(calcd), g/cm^3	1.648	1.504	1.618	1.661	1.709	1.821	1.642	1.671	1.579	1.73	1.533
μ, mm^{-1}	0.168	0.173	0.188	0.262	1.382	1.206	0.387	0.422	0.348	0.689	1.12
$T_{min}-T_{max}$	0.950 72−0.988 77	0.9377−0.9789	0.952 08−0.987 57	0.944 86−0.975 04	0.677 36−0.907 08	0.695 67−0.909 04	0.898 68−0.969 38	0.727 662−0.989[b]	0.905 79−0.987 20	0.890 11−0.973 67	0.7043 −0.9685
no. of measd rflns	22 657	46 426	35 713	28 960	20 514	45 529	36 465	35 163	46 991	19 679	15 514
no. of indep rflns	11 546	23 459	18 073	7880	7855	12 345	18 343	9362	23 912	5285	11 048
no. of rflns $>2\sigma(I)$	4419	12242	8474	5488	4050	6283	10461	6755	5929	3021	5220
R_{int}	0.1749	0.1399	0.1505	0.0688	0.1278	0.1278	0.1045	0.0747	0.3386	0.1234	0.1687
$R[F^2 > 2\sigma(F^2)]$	0.0678	0.0815	0.0750	0.0450	0.0484	0.0490	0.0507	0.0463	0.1069	0.0615	0.089
$R_w(F^2)$	0.2292	0.2808	0.2660	0.1249	0.1402	0.1401	0.1476	0.136	0.2752	0.1814	0.3004
S	0.879	1.018	1.028	1.034	0.932	0.961	0.973	1.089	0.877	0.981	0.967
no. of params	777	1433	1135	487	487	793	1143	582	1406	309	659

[a] Conditions: CCD area detector diffractometer; ψ and ω scans; temperature for data collection 153(2) K; Mo Kα radiation; $\lambda = 0.710\ 73$ Å. [b] Estimated from crystal diffraction data, with T_{min}/T_{max} calculated using SADABS.

Scheme 1

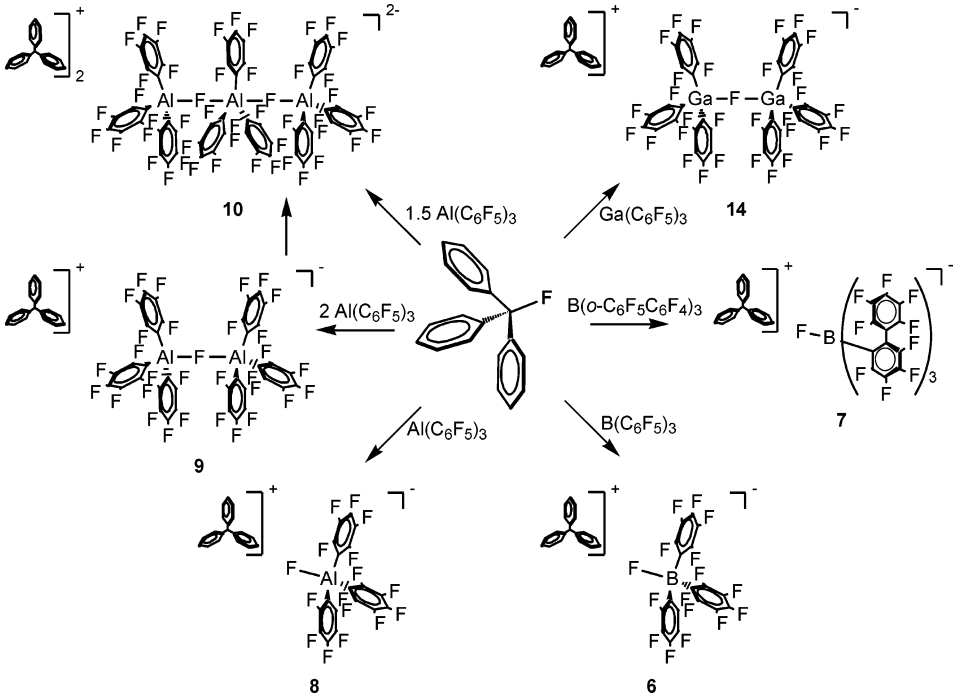

Table 2. Comparison of Selected Bond Distances (Å) for Cocatalysts 4, 7, and 11−14

	4	**7**	**10**		**11**		**12**	**13**	**14**
	$FAl(o\text{-}C_6F_5\text{-}C_6F_4)_3$	$FB(o\text{-}C_6F_5\text{-}C_6F_4)_3$	Al−F−Al−F−Al		$(C_6F_5)_3AlFAl\text{-}(o\text{-}C_6F_5C_6F_4)_3$		$ClAl(C_6F_5)_3$	$BrAl(C_6F_5)_3$	Ga−F−Ga
M−X	1.682(5)	1.437(6)	1.738(3)[b,d]	1.965(2)[e]	1.770(3)[f]	1.797(3)[g]	2.1676(7)	2.3317(18)	1.907(2)[b]
$M-C_{aryl}$[b]	2.018(6)	1.654(6)	1.999(4)[d]	2.003(4)[e]	1.983(5)[f]	2.008(4)[g]	2.007(4)	2.006(8)	1.990(4)
$C-C_{phenyl}$[c]	1.44(1)	1.443(6)	1.447(6)		1.439(6)		1.445(3)	1.440(6)	1.447(5)

[a] X = F, Cl, or Br. [b] Average of bond distance. [c] Average of bond distance in trityl cation. [d] $F-Al_{terminal}$. [e] $F-Al_{internal}$. [f] $FAl(C_6F_5)_3$. [g] $FAl(o\text{-}C_6F_5C_6F_4)_3$.

structural, and reactivity data present a unique opportunity for an in-depth comparitive analysis of these metalloid−halogen interactions.

II. Activation of Metallocene $Me_2C(Cp)(Flu)ZrMe_2$ (15) with Cocatalysts 6−14. General Considerations. Activation of typical group 4 metallocene dimethyls with methide-abstracting cocatalyst reagents is observed to generate highly reactive metallocenium perfluoroarylmetalate complexes that typically exist as contact ion pairs in nonpolar media, even at catalytic ($<10^{-4}$ M) concentrations.[10,11] Complex mixtures and decomposition products are often observed as well, especially with highly active polymerization catalyst systems studied in the absence of olefin.

The study of activation reactions using a broad array of precatalyst and cocatalyst species has led to the identification of a number of different modes of cation−anion interactions. These observations, coupled with profound observed anion-dependent effects on the relative rates of various enchainment, misinsertion, reorganization, and termination processes, have led to an emergent picture in which the mode and strength of ion pairing plays a significant role in determining polymerization activity and stereoselectivity.

Metallocene-derived cations have been observed in both mononuclear or dinuclear configurations (e.g., having single μ-methyl linkages between metal centers, see eq 2).[1] In some cases, either product or a mixture of both is possible—as with the cocatalyst $Ph_3C^+B(C_6F_5)_4^-$—depending on the reaction conditions, stoichiometry, metallocene ancillary ligation, solvent, etc.[22] Both mononuclear and dinuclear monocations have been reported in the reactions of **15** with various cocatalyst reagents. The anion may also be mono- or polynuclear and can interact with the cation either via specific interatomic contacts or in the absence of any dominant low-energy interatomic contact. For

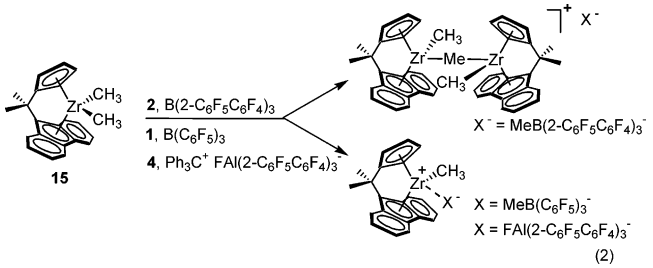

(2)

example, the cocatalyst reagents $B(C_6F_5)_3$ (**1**) and $Ph_3C^+FAl(o\text{-}C_6F_5C_6F_4)_3^-$ (**4**) afford contact ion pairs having a mononuclear zirconocenium cation with the anion occupying a vacancy in the Zr coordination sphere and interacting with the cationic Zr center via a μ-methyl or μ-fluoro linkage,[12] while the sterically encumbered mononuclear cocatalyst $B(o\text{-}C_6F_5C_6F_4)_3$ (**2**) yields a contact ion pair having a dinuclear bridged monocation with the μ-methyl group completing the coordination spheres of both Zr centers and a nonspecific cation−anion contact (eq 2).[9a] The exact fates of such alkyl-bridged dinuclear species during olefin polymerization processes remain unclear.[23]

The persistence of particular modes of cation−anion interaction during polymerization reactions remains an area of intensive study. Interestingly, the cation−anion interaction can be quite kinetically inert and still mediate polymerization: whereas in

(22) Al-Humydi, A.; Garrison, J. C.; Youngs, W. J.; Collins, S. *Organometallics* **2005**, *24*(2), 193−196. (b) Lancaster, S. J.; Bochmann, M. *J. Organomet. Chem.* **2002**, *654*, 221−223.

Scheme 2

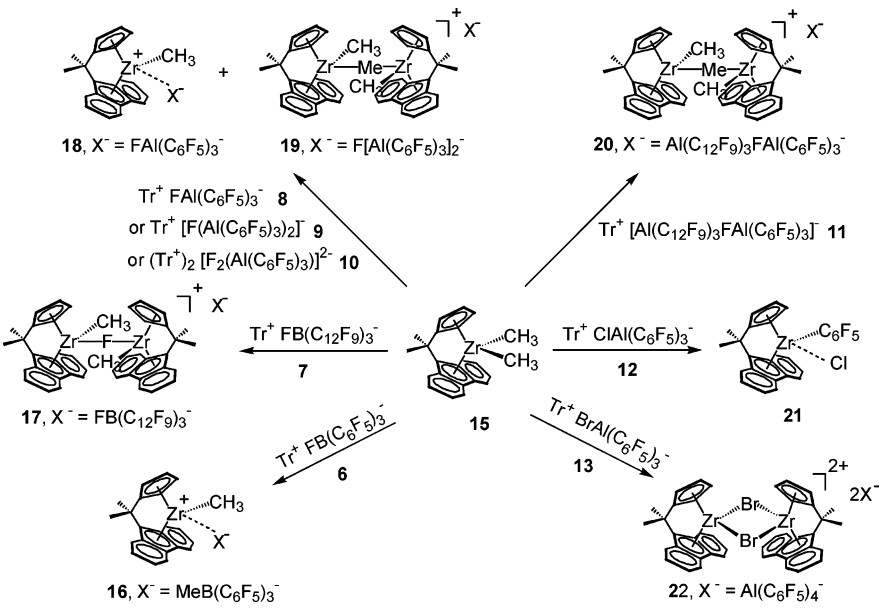

complex **16** the cation−anion interaction is observed to be rather labile, in mononuclear $Me_2C(Cp)(Flu)ZrMe^+FAl(o\text{-}C_6F_5C_6F_4)_3^-$ (generated from **15** + **4**), the $FAl(o\text{-}C_6F_5C_6F_4)_3^-$ anionic fragment coordinates to the metal center via an exceptionally robust Zr−F−Al linkage, strongly attenuating or shutting down solution-phase unimolecular catalyst epimerization, as observed in isolation, while still permitting propylene enchainment under polymerization conditions.[12] Halide linkages of this type have also been observed in the reaction of AlR_3 reagents with metallocene halides.[24] The possibility of accessing new variants of this bonding motif, and entirely new ion-pair structures, has motivated the synthesis/development of new cocatalysts **6**−**14** and the study of their reactions with the archetypal $Me_2C(Cp)(Flu)ZrMe_2$ (**15**).

Beyond differences in spectroscopic and structural characteristics, the present B-, Al-, and Ga-based systems can be differentiated by their activation chemistry. Cocatalysts **6**−**14** all react with metallocene **15**, in some cases generating highly active olefin polymerization catalyst ion pairs; polymerization results are presented in a companion report.[17] As monitored by in situ NMR spectroscopy, reaction via trityl cation abstraction of one metallocene methide ligand is rapid in all cases and appears to proceed to completion, on the basis of the observed evolution of 1.0 stoichiometric equiv of triphenylethane. Many of the resultant mixtures are complicated, with multiple products observed; spectroscopically identified products are shown in Scheme 2. Exhaustive attempts were made to isolate single-crystal samples from each of these reaction mixtures, and three new ion-pair complexes and two decomposition products have been characterized by single-crystal X-ray diffraction (see below).

III. Trityl (Perfluoroaryl)Fluoroborates $Ph_3C^+FB(C_6F_5)_3^-$ (6) and $Ph_3C^+FB(o\text{-}C_6F_5C_6F_4)_3^-$ (7). The reaction of trityl fluoride[18] with $B(C_6F_5)_3$ (**1**) and $B(o\text{-}C_6F_5C_6F_4)_3$ (**2**) [5a] yields the corresponding trityl fluorometalate salts, trityl tris(perfluorophenyl)fluoroborate (**6**: 68%; eq 3)[25] and trityl tris(2,2′,2″-nonafluorobiphenyl)fluoroborate (**7**: 63%; eq 4). Bridged

$$\underset{\mathbf{1}}{PhCF} + B(C_6F_5)_3 \rightarrow \underset{\mathbf{6}}{Ph_3C^+\ FB(C_6F_5)_3^-} \qquad (3)$$

$$\underset{\mathbf{2}}{Ph_3CF} + B(C_{12}F_9)_3 \rightarrow \underset{\mathbf{7}}{Ph_3C^+\ FB(o\text{-}C_6F_5C_6F_4)_3^-} \qquad (4)$$

B−F−B species are not observed. In addition to sharp fluoroaryl signals, the ^{19}F NMR spectra of both fluoroborates exhibit characteristic broad, upfield B−*F* resonances at δ −186.99 (**6**) and −185.00 ppm (**7**). Integration of these resonances versus the fluoroaryl resonances is consistent with the molecular structures proposed for **6** and **7**.

The crystal structure of complex **7** has also been confirmed by X-ray diffraction and features an unassociated trityl cation and a sterically congested chiral, essentially C_3-symmetric borate anion, as shown in Figure 1. Selected bond distances and angles are summarized in Table 3. The anion in **7** adopts a pseudotetrahedral geometry, and the B−F distance (1.437(6) Å) and average $B-C_{aryl}$ distances (1.654(6) Å) are not unexpectedly shorter than the corresponding Al−F (1.682(5) Å) and $Al-C_{aryl}$ (2.018(9) Å) distances in the homologous Al cocatalyst **4**.[9a] The Al−F and B−F bond distances are within 3% of the summed Shannon ionic radii but are considerably smaller than the summed covalent radii, whereas the $B-C_{aryl}$ and $Al-C_{aryl}$ distances closely match the corresponding summed covalent radii.[26] As with **4**, the biphenyl groups of **7** encapsulate the metalloid-bound fluorine atom, and the fluoroaryl rings in the

(23) Direct NMR observation of mononuclear and dinuclear catalyst polymeryl species suggests that the concentration of methyl-bridged dinuclear species can diminish in the presence of olefin and that such species may constitute resting states under certain conditions; see: Tritto, I.; Donetti, R.; Sacchi, M. C.; Locatelli, P.; Zannoni, G. *Macromolecules* **1999**, *32*, 264−269.

(24) (a) Activation of $(Cp^*TiOF)_4$ with $AlMe_3$ affords $(Cp^*TiO)_4(FAlMe_3)_4$: Yu, P. H.; Roesky, H. W.; Demsar, A.; Albers, T.; Schmidt, H. G.; Noltemeyer, M. *Angew. Chem., Int. Ed. Engl.* **1997**, *36*, 1766−1767. (b) Activation with $Al(CH_2Ph)_3(Cp^*TiO)_4(F)_3[FAl(CH_2Ph)_3]$: Yu, P.; Pape, T.; Usón, I.; Said, M. A.; Roesky, H. W.; Montero, M. L.; Schmidt, H.-G.; Demsar, A.. *Inorg. Chem.* **1998**, *37*, 5117−5124. (c) Reaction of Cp_2TiF_2 with $AlEt_3$ gives $[Cp_2Ti(\mu_2\text{-}F)_2AlEt_2]_2$: Yu, P.; Montero, M. L.; Barnes, C. E.; Roesky, H. W.; Usón, I. *Inorg. Chem.* **1998**, *37*, 2595−2597. (d) For reaction of Cp_2ZrMe_2 with $[(Me_3Si)_3CAlF_2]_3$ and Me_3SnF, see Hatop, H.; Roesky, H. W.; Labahn, T.; Fischer, A.; Schmidt, H. G.; Noltemeyer, M. *Organometallics* **2000**, *19*, 937−940.

(25) The similar fluoroborate $Li^+FB(C_6F_5)_3^-$ has been claimed previously. See: Klemann, L. P.; Newman, G. H.; Stogryn, E. L. U.S. Patent 4,139,681, 1979.

(26) For ionic radii, see: (a) Shannon, R. D. *Acta Crystallogr.* **1976**, *A32*, 751−767. For covalent radii, see: (b) Huheey, J. E.; Keiter, E. A.; Keiter, R. L. In *Inorganic Chemistry: Principles of Structure and Reactivity*, 4th ed.; HarperCollins: New York, 1993.

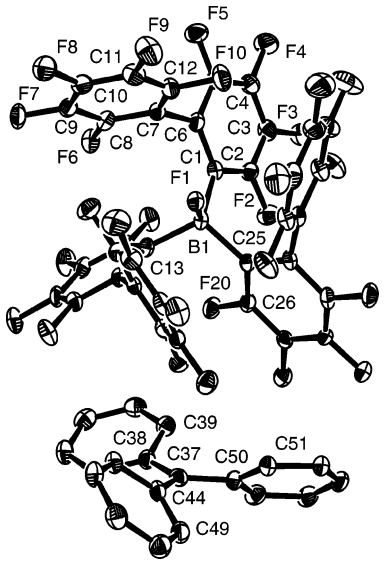

Figure 1. Perspective ORTEP drawing of the molecular structure of the cocatalyst reagent $Ph_3C^+FB(o\text{-}C_6F_5C_6F_4)_3^-$ (**7**). Thermal ellipsoids are drawn at the 30% probability level.

Table 3. Selected Bond Distances and Angles for the Cocatalyst $Ph_3C^+FB(o\text{-}C_6F_5C_6F_4)_3^-$ (7)

Bond Distances (Å)			
B1−F1	1.437(6)	C18−C19	1.495(6)
B1−C1	1.649(7)	C30−C31	1.477(6)
B1−C25	1.655(6)	C37−C38	1.425(6)
B1−C13	1.659(6)	C37−C44	1.442(6)
C6−C7	1.504(6)	C37−C50	1.463(6)
Bond Angles (deg)			
F1−B1−C1	105.3(4)	C38−C37−C44	121.8(4)
F1−B1−C13	106.8(3)	C38−C37−C50	120.6(4)
F1−B1−C25	107.2(3)	C44−C37−C50	117.4(4)
C1−B1−C13	114.4(4)	C1−C6−C7	123.4(4)
C1−B1−C25	112.2(3)	C13−C18−C19	123.4(4)
C25−B1−C13	110.4(4)	C25−C30−C31	123.4(4)
Torsion Angles (deg)			
C1−C6−C7−C8		−77.9	
C13−C18−C19−C24		−94.9	
C25−C30−C31−C36		−81.4	

biphenyl groups are substantially twisted out of coplanarity (−84.7° (average); vide infra for a discussion of perfluorobiphenyl configuration effects).

The activation reactions of the metallocene $Me_2C(Cp)(Flu)ZrMe_2$ (**15**) with cocatalysts **6** and **7** are rapid, with B−F bond cleavage observed in both cases: **6** + **15** affords $Me_2C(Cp)(Flu)ZrMe^+MeB(C_6F_5)_3^-$ (**16**, also produced via reaction of **15** with **1**) in 30% yield,[27] implying formation of an insoluble zirconocene fluoride side product (putatively, $[Me_2C(Cp)(Flu)ZrMeF]_n$; see eq 5). No ^{19}F signal consistent with a B−F or Zr−F environment is observed. For the cocatalyst reagent $Ph_3C^+FB(o\text{-}C_6F_5C_6F_4)_3^-$ (**7**), dinuclear $[Me_2C(Cp)(Flu)ZrMe]_2(\mu\text{-}F)^+FB(o\text{-}C_6F_5C_6F_4)_3^-$ diastereomers (**17**) form in a 2:1 ratio by NMR (**B** and **C**). The sequence outlined in eq 6 suggests possible pathways for the formation of **17**. In the ^{19}F NMR, nine distinct fluoroaryl ^{19}F signals are observed, indicating

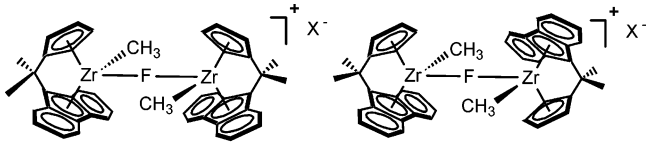

B **C**

17, $X^- = FB(o\text{-}C_6F_5C_6F_4)_3^-$

restricted internal fluoroaryl ring rotation. The Zr−*F*−Zr and *F*−B ^{19}F signals of the ion pair **17** appear as broad singlets at

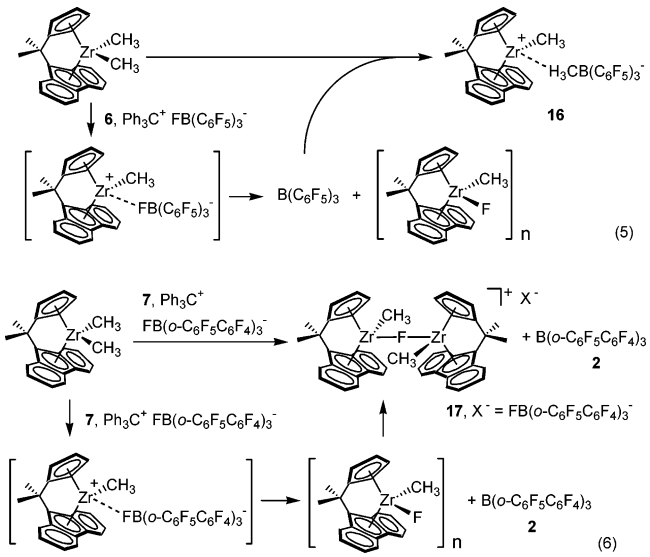

δ −77.97 and −184.47 ppm, respectively, the latter being similar to the *F*−B signal in **7** (δ −185.00 ppm). These signals exhibit a 1:1 integral ratio and a 1:3 ratio versus the sum of fluoroaryl signal integrals, consistent with the proposed solution structures for diastereomers **17**.[16] The zirconocene dimethyl and cocatalyst trityl salt are combined in a 1:1 ratio to generate **17**; free $B(o\text{-}C_6F_5C_6F_4)_3$ is also observed in ∼50% yield in the crude reaction mixture, again indicating a B−F bond cleavage event (eq 6) and suggesting a source for the bridging fluoride in the cationic fragments of **17**. Added cocatalyst **7** beyond 1.0 equiv remains unreacted at room temperature.

The crystal structure of complex **17** has been confirmed by X-ray diffraction and features an unassociated, F-bridged dinuclear Zr−F−Zr cation and a sterically congested pseudo-tetrahedral fluoroborate anion (Figure 2). Selected bond distances and angles are summarized in Table 4. The overall structure of the anion in **17** is quite similar to that of trityl salt **7**: in particular, the B−F distances for for **7** and **17** are quite close (1.424(5) and 1.437(6) Å, respectively), and the averaged $B-C_{aryl}$ distances are indistinguishable (1.661(5) vs 1.654(6) Å). The perfluorobiphenyl substituents again encapsulate the F atom (vide infra, and see Table 8 for a detailed comparison of observed perfluorobiphenyl ligand arrangements). The marked similarity in ^{19}F spectra for **7** and **17** suggest that these similarities persist in solution: i.e., that the cation−anion interaction is not mediated by a Zr−F−B linkage (a profound Zr-induced ^{19}F chemical shift effect is seen in the analogous zirconocenium fluoroaluminates having Zr−F−Al linkages; vide infra).

The observed B−F bond cleavage chemistry, along with an absence of any structural or NMR evidence for Zr−F−B or B−F−B species, suggests that (a) such a bridging structure may be unstable in the present context[28] and (b) the Zr−F−Zr linkage is stronger than a possible Zr−F−B linkage—the neutral $Me_2C(Cp)(Flu)ZrMeF$ moiety can be viewed as outcompeting the anion for coordination to the $Me_2C(Cp)(Flu)ZrMe^+$ moiety in this case. In contrast, F−Al bond cleavage is not observed in the reaction of **15** with the fluoroaluminate reagent **4**, the

(27) The other product is an unidentified precipitate which exhibits very broad peaks in the ^1H NMR (CD_2Cl_2), and the structural identification is ambiguous. However, examples of Zr−F formation in catalyst deactivation processes have been observed previously.[1c,9a,24]

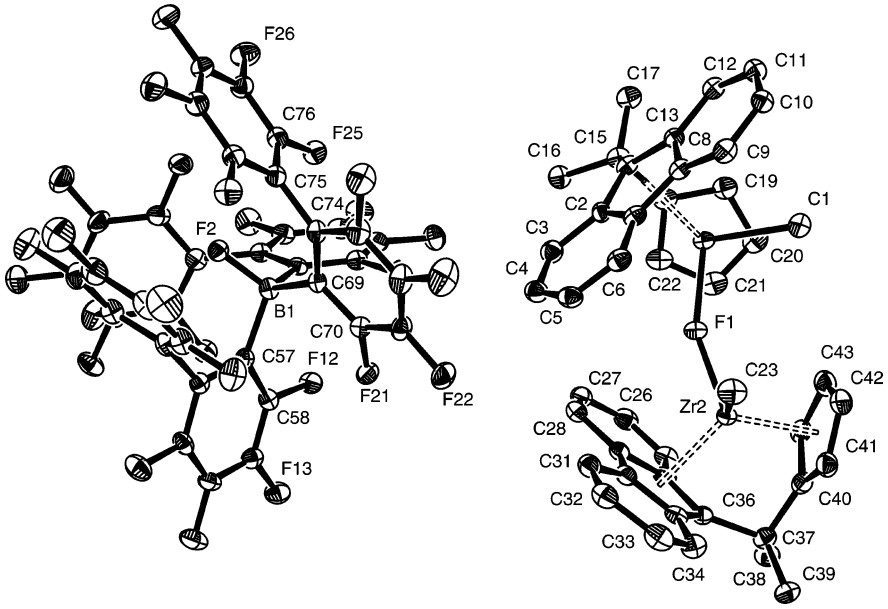

Figure 2. Perspective ORTEP drawing of the molecular structure of the dinuclear Zr−(μ-F)−Zr complex $[Me_2C(Cp)(Flu)ZrMe]_2(\mu\text{-}F)^+FB(o\text{-}C_6F_5C_6F_4)_3^-$ (**17**). Thermal ellipsoids are drawn at the 30% probability level.

Table 4. Selected Bond Distances and Angles for the Dinuclear Metallocene Complex $[Me_2C(Cp)(Flu)ZrMe]_2(\mu\text{-}F)^+FB(o\text{-}C_6F_5C_6F_4)_3^-$ (17)

Bond Distances (Å)			
C1−Zr1	2.257(4)	B1−C57	1.653(6)
C23−Zr2	2.248(4)	Zr1−Flu_{cent}[a]	2.231
B1−F2	1.424(5)	C15−C18	1.541(6)
C62−C63	1.487(5)	C37−C40	1.523(6)
F1−Zr1	2.095(2)	B1−C69	1.664(5)
F1−Zr2	2.103(2)	Zr2−Cp_{cent}[a]	2.175
B1−C45	1.666(5)	Zr1− C15	3.137
Zr−Cp_{cent}	2.166	Zr2− C37	3.107
C14−C15	1.555(5)	C50−C51	1.501(6)
C36−C37	1.546(6)	Zr2−Flu_{cent}	2.225

Bond Angles (deg)			
Zr1−F1−Zr2	155.57(12)	C18−C15−C14	98.6(3)
F2−B1−C45	106.5(3)	C40−C37−C36	99.8(3)
F2−B1−C57	108.0(3)	C45−B1−C69	113.4(3)
F2−B1−C69	107.7(3)	C57−C62−C63	122.0(3)
F1−Zr1−C1	98.35(13)	Cp_{cent}−Zr1−Flu_{cent}	118.6
F1−Zr2−C23	92.60(13)	Cp_{cent}−Zr2−Flu_{cent}	119.0
C45−B1−C57	112.0(3)	C57−B1−C69	109.1(3)
C45−C50−C51	123.5(3)	C69−C74−C75	124.3(3)

Torsion Angles (deg)	
C45−C50−C51−C52	−94.4
C-57-C62−C63−C64	−97.9
C69−C74−C75−C76	−59.7

[a] Centroid of C_5 ligand.

perfluorobiphenyl ligands rearranging to accommodate a Zr−F−Al linkage.[12a]

Diffraction data for **17** are of sufficient quality to unambiguously identify the bridging moiety as μ-F rather than μ-CH_3 in this structure, with bond lengths consistent with the suggested atom assignment. The cation in **17** has a bent Zr−F−Zr configuration, with the F atom equidistant from both Zr atoms (see Table 4). Three similar fluoride-bridged dinuclear Zr−F−Zr cationic structures, $[(Cp''_2ZrMe)_2(\mu\text{-}F)]^+MeB(C_6F_5)_3^-$ (**D**),[4a] $[(Cp''_2ZrF)_2(\mu\text{-}F)]^+B[o\text{-}C_6F_4(i\text{-}C_3H_7)]_4^-$ (**E**),[7b] and $[Me_2C(Cp)(Flu)Zr(C_6F_5)]_2(\mu\text{-}F)^+MeB(C_6F_5)_3^-$ (**F**),[9a] have been previously

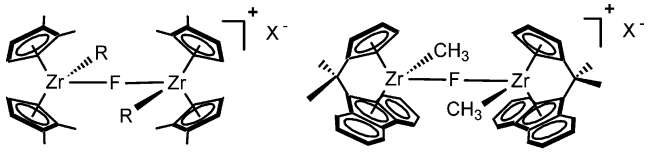

D, $X^- = CH_3B(C_6F_5)_3^-$, R = CH_3 **F**, $X^- = CH_3B(C_6F_5)^-$

E, $X^- = B[o\text{-}C_6F_4(i\text{-}C_3H_7)]_4^-$, R = F

reported, all obtained as decomposition products from metallocene−borane ion pairs. Table 5 compares relevant bond distances and angles for these four Zr−F−Zr cations. Among these, complex **17** presents the shortest Zr−(μ-F) bond distance (2.099(4) Å, average) and the most acute Zr−(μ-F)−Zr bond angle (155.57(13)°), thus having the shortest Zr···Zr distance (4.103 Å).

IV. A. Trityl Perfluoroaryl Fluoroaluminates $(Ph_3C^+)_x F_x[Al(C_6F_5)_3]_y^{x-}$ ($x = 1, y = 1$, **8; $x = 1, y = 2$, **9**; $x = 2, y = 3$, **10**) and $Ph_3C^+(C_6F_5)_3AlFAl(o\text{-}C_6F_5C_6F_4)_3^-$ (**11**).** Natta et al. have shown that the bimetallic, fluorine-bridged $F[AlEt_3]_2^-$ anion can be generated as a potassium salt using a 1:2 ratio of KF and $AlEt_3$.[29] Combining trityl fluoride and $Al(C_6F_5)_3$ (**3**) gives similar results: depending on the reagent molar ratio, any of the three trityl tris(perfluorophenyl) fluoroaluminates $(Ph_3C^+)_xF_x[Al(C_6F_5)_3]_y^{x-}$ ($x = 1$, $y = 1$, **8**; $x = 1$, $y = 2$, **9**; $x = 2$, $y = 3$, **10**) can be isolated in good yield (eqs 7−10).

$$\underset{\mathbf{3}}{Ph_3CF} + Al(C_6F_5)_3 \rightarrow \underset{\mathbf{8}}{Ph_3C^+[FAl(C_6F_5)_3]^-} \quad (7)$$

$$\underset{\mathbf{3}}{Ph_3CF} + 2Al(C_6F_5)_3 \rightarrow \underset{\mathbf{9}}{Ph_3C^+F[Al(C_6F_5)_3]_2^-} \quad (8)$$

$$\underset{\mathbf{3}}{2Ph_3CF} + 3Al(C_6F_5)_3 \rightarrow \underset{\mathbf{10}}{(Ph_3C^+)_2\,F_2[Al(C_6F_5)_3]_3^{2-}} \quad (9)$$

$$\underset{\mathbf{4}}{Ph_3C^+[FAl(o\text{-}C_6F_5C_6F_4)_3]^-} + \underset{\mathbf{3}}{Al(C_6F_5)_3} \rightarrow \underset{\mathbf{11}}{Ph_3C^+(C_6F_5)_3AlFAl(o\text{-}C_6F_5C_6F_4)_3^-} \quad (10)$$

(28) B−F−B linkages have been seen in three solid-state structures containing a $F[BF_3]_2^-$ anion: (a) Watanabe, M.; Sato, M.; Nagasawa, A.; Kai, M.; Motoyama, I.; Takayama, T. *Bull. Chem. Soc. Jpn.* **1999**, *72*, 715. (b) Akiba, K.; Yamashita, M.; Yamamoto, Y.; Nagase, S. *J. Am. Chem. Soc.* **1999**, *121*, 10644. (c) Braunstein, P.; Douce, L.; Fischer, J.; Craig, N. C.; Goetz-Grandmont, G.; Matt, D. *Inorg. Chim. Acta* **1992**, *194*, 151. A neutral, structurally asymmetric (fluoro)borabicyclononane dimer with one tetrahedral B and one planar B atom has also been reported: Koster, R.; Schussler, W.; Boese, R. *Chem. Ber.* **1990**, *123*, 1945.

Table 5. Comparison of Selected Bond Distances (Å) and Angles (deg) for Dinuclear Metallocene Cations Containing Zr−F−Zr Linkages

	[Zr]−F−[Zr]			
	D[4a]	**E**[7b]	**F**[9a]	**17**
[Zr]	1,2-Me_2CpZrMe	1,2-Me_2CpZrF	Me_2C(Cp)(Flu)Zr(C_6F_5)	Me_2C(Cp)(Flu)ZrMe
anion	$MeB(C_6F_5)_3^-$	$B(C_6F_4(C_3H_7))_4^-$	$MeB(C_6F_5)_3^-$	$FB(o\text{-}C_6F_5C_6F_4)_3^-$
Zr−(μ-F)[a]	2.113(5)	2.111(2)	2.152(2)	2.099(4)
Zr−R[b]	2.222(3)	1.934(13)	2.306(2)	2.253(5)
Zr−(μ-F)−Zr[c]	173.3(1)	158.0(6)	174.3(3)	155.57(13)
R−Zr−(μ-F)[d]	93.8(20)	94.0(13)	106.3(6)	95.5(31)
Cp_{cent}−Zr−Cp_{cent}[e]	131.3(5)	131.4(5)	118.1(1)	118.8(2)
R−Zr−Zr−R[f]	99.9	96.4	89.2	67.1
Zr−Zr[g]	4.219	4.144	4.300	4.103

[a] Mean bond distance. [b] Mean Zr−R bond distance, R = Me, C_6F_5 (in **F**) or R = F (in **E**). [c] Bond angle. [d] Mean R−Zr−(μ-F) bond angle. [e] Centroid of C_5 ligand. [f] Torsion angle. [g] Metal−metal distance.

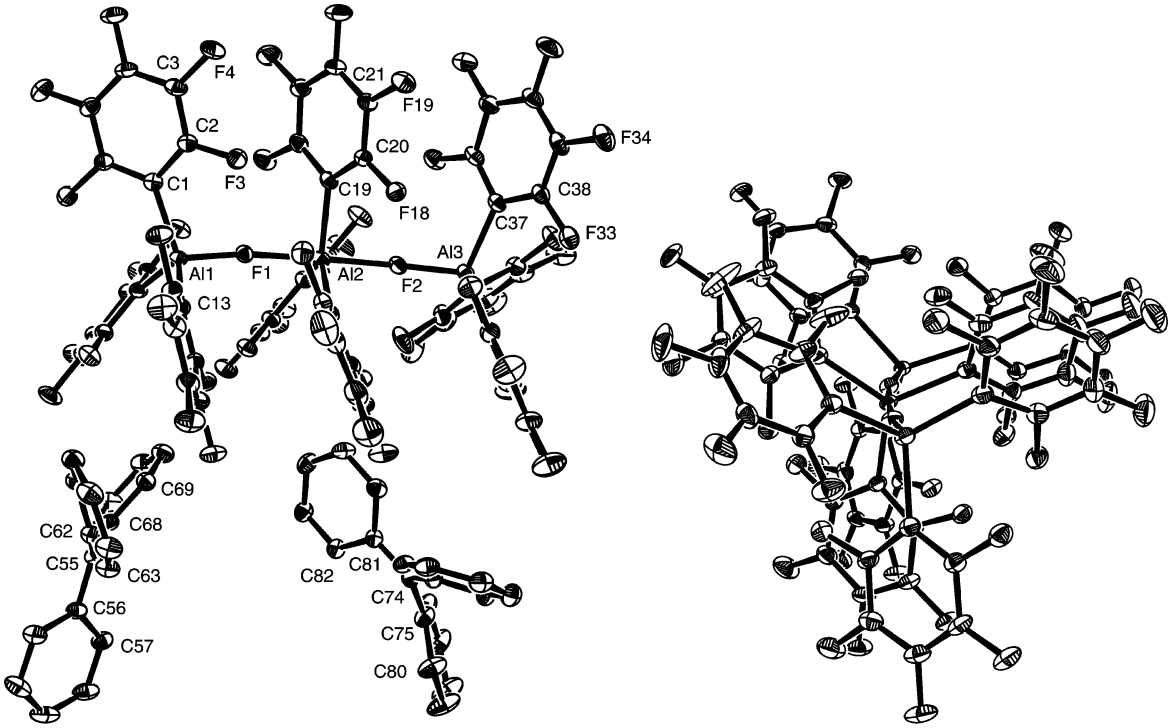

Figure 3. Perspective ORTEP drawings of the molecular structure of the cocatalyst reagent $(Ph_3C^+)_2F_2[Al(C_6F_5)_3]_3^{2-}$ (**10**) (A) viewed perpendicular to the (noncrystallographic) Al−F−Al−F−A1 axis and (B) viewed along this axis. Thermal ellipsoids are drawn at the 30% probability level.

Fluoroaluminate **10** was characterized by single-crystal X-ray diffractometry (Figure 2; see below).

The ^{19}F NMR spectra of complexes **8**−**10** exhibit broad singlets at δ −168.61, −167.30, and −166.49, respectively. In comparison to the *F*−Al signal of $Ph_3C^+FAl(C_6F_5)_3^-$ (**8**), the Al−*F*−Al resonance of dinuclear $Ph_3C^+F[Al(C_6F_5)_3]_2^-$ (**9**) is shifted slightly downfield by the additional F-coordinated Al-$(C_6F_5)_3$ moiety. In this case, it appears that any diamagnetic shielding of the bridging F nucleus due to heightened steric congestion in **9** is outweighed by the electron-withdrawing effect of the added, strongly Lewis acidic fragment. Similarly, the Al-$(F-Al)_2$ signal in trinuclear **10** appears slightly downfield of the Al−*F*−Al resonance dinuclear **9**. Perfluorophenyl ^{19}F chemical shift differences between **8** and **9** are small ($\Delta\delta$ = +0.14, +1.77, and +0.38 ppm for *o*-, *m*-, and *p*-F atoms, respectively). The perfluorophenyl ^{19}F NMR signals for **10** are also quite similar to those of **8** and **9**. Notably, the C_6F_5 ^{19}F resonances of the terminal and bridging $Al(C_6F_5)_3$ moities in **10** are within ±0.09 and ±0.94 ppm of the corresponding values for **9**, respectively.

The solid-state structure of complex **10** features two unassociated trityl cations and a sterically congested pseudo-C_3-symmetric trinuclear anion where the three Al centers are connected by two μ-F atoms in a nearly linear Al−F−Al−F−Al configuration (Figure 3; selected bond distances and angles are summarized in Table 6).[30] The average $F-Al_{terminal}$ distance (1.738(3) Å) is noticeably shorter than the average $F-Al_{internal}$ distance (1.965(2) Å), and the bridging Al atom has a trigonal-bipyramidal coordination geometry, whereas the terminal Al atoms exhibit distorted-tetrahedral coordination geometries. The

(29) For the first structural study of a fluoro-bridged organoaluminum complex, $K^+F[AlEt_3]^-$, with F−Al = 1.80(6) Å, see: Natta, G.; Allegra, G.; Perego, G.; Zambelli, A. *J. Am. Chem. Soc.* **1961**, *83*, 5033.

(30) A similar M−F−M−F−M arrangement has been observed in a Bi system. For a recent review of such metal fluorides, see: Roesky, H. W.; Haiduc, I. *J. Chem. Soc., Dalton Trans.* **1999**, *14*, 2249−2264.

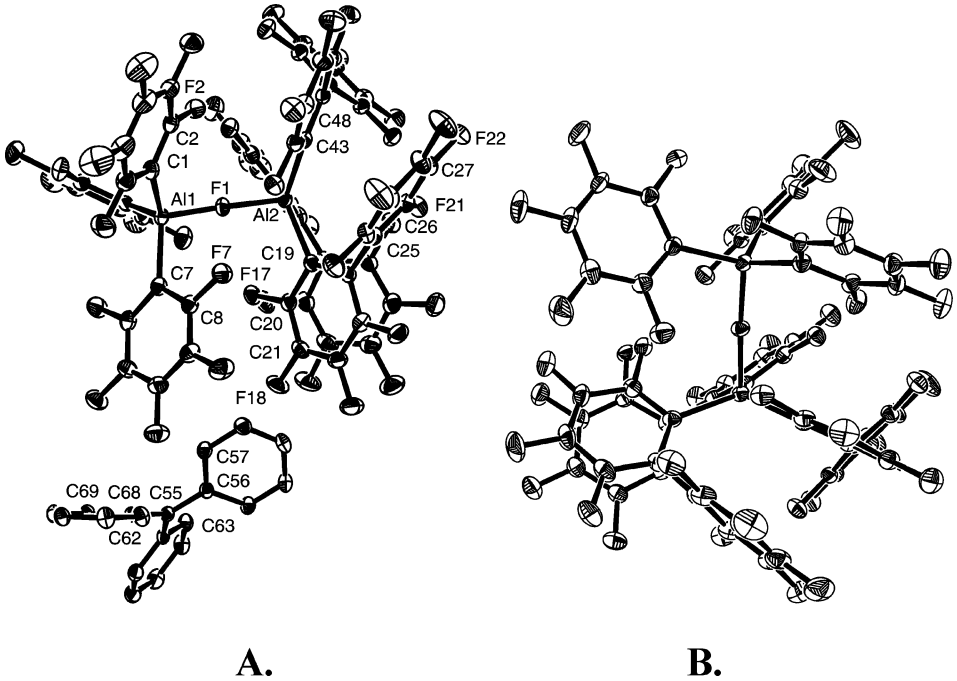

Figure 4. Perspective ORTEP drawings of the molecular structure of the cocatalyst reagent $Ph_3C^+(C_6F_5)_3AlFAl(o\text{-}C_6F_5C_6F_4)_3^-$ (**11**) (A) viewed across the Al−F−Al axis and (B) viewed showing mutual $\pi-\pi$ or steric stacking among the $o\text{-}C_6F_5C_6F_4$ groups. Thermal ellipsoids are drawn at the 30% probability level.

Table 6. Selected Bond Distances (Å) and Angles (deg) for the Cocatalyst $(Ph_3C^+)_2F_3[Al(C_6F_5)_3]_3^{2-}$ (10)

Bond Distances (Å)			
Al1−F1	1.741(2)	Al3−C37	1.999(4)
Al1−C1	2.000(4)	Al3−C43	1.995(4)
Al1−C13	1.986(4)	Al3−C49	2.003(5)
Al1−C7	2.008(4)	C55−C56	1.443(5)
Al2−F1	1.964(2)	C55−C62	1.458(6)
Al2−F2	1.965(2)	C55−C68	1.440(6)
Al2−C19	1.996(4)	C74−C75	1.446(6)
Al2−C25	2.009(4)	C74−C81	1.449(6)
Al2−C31	2.004(4)	C74−C87	1.438(6)
Al3−F2	1.734(3)		
Bond Angles (deg)			
Al1−F1−Al2	168.56(15)	C19−Al2−C25	117.04(17)
Al3−F2−Al2	173.51(15)	C19−Al2−C31	120.77(17)
F1−Al1−C1	106.38(14)	C25−Al2−C31	122.19(17)
F1−Al1−C7	104.85(15)	F2−Al3−C37	104.77(15)
F1−Al1−C13	105.36(15)	F2−Al3−C43	105.71(15)
C1−Al1−C7	110.36(17)	F2−Al3−C49	107.54(15)
C1−Al1−C13	115.48(17)	C37−Al3−C43	112.04(17)
F1−Al2−F2	177.03(12)	C37−Al3−C49	113.79(18)
F1−Al2−C19	89.62(14)	C43−Al3−C49	112.26(17)
F1−Al2−C25	91.05(14)	C56−C55−C62	118.0(4)
F1−Al2−C31	89.73(14)	C56−C55−C68	121.9(4)
F2−Al2−C19	91.16(14)	C62−C55−C68	120.1(3)
F2−Al2−C25	91.15(14)	C75−C74−C81	119.8(4)
F2−Al2−C31	87.41(14)	C75−C74−C87	118.7(4)

$Al-C_{aryl}$ distances for bridging and terminal Al atoms in **10** are indistinguishable (1.999(4) and 2.003(4) Å, respectively) and are comparable to $Al-C_{aryl}$ distances in cocatalysts **4** and **11**−**14** (see Table 2 for a detailed comparison of the seven cocatalysts). The three sets of fluoroaryl rings are substantially eclipsed, and in each set the fluoroaryl moieties are twisted out of the equatorial plane (Figure 3A), suggesting strong $\pi-\pi$ or steric interactions among the three sets of fluoroaryl rings (Figure 3B).

The previously isolated monometallic trityl salt $Ph_3C^+FAl(o\text{-}C_6F_5C_6F_4)_3^-$ (**4**) [9a] undergoes reaction with $Al(C_6F_5)_3$ to afford the fluoro-bridged mixed aluminate $Ph_3C^+(C_6F_5)_3AlFAl(o\text{-}C_6F_5C_6F_4)_3^-$ (**11**; eq 7). Neutral $Al(o\text{-}C_6F_5C_6F_4)_3$ and thus the symmetrically bridged $Ph_3C^+F[Al(o\text{-}C_6F_5C_6F_4)_3]_2^-$ are synthetically inaccessible by the present methods. Fluoroaluminate **11** was also characterized by single-crystal X-ray diffractometry (Figure 4; see below).

The effect of $Al(C_6F_5)_3$ coordination to the $FAl(o\text{-}C_6F_5C_6F_4)_3^-$ anion in the trityl salt **4** is quite significant compared to that of $Al(C_6F_5)_3$ coordination to the $FAl(C_6F_5)_3^-$ anion in the trityl salt **8**, according to the ^{19}F NMR data: the chemical shift difference between the Al-bound F atoms of mononuclear **4** (δ −175.02 ppm)[31] and asymmetric dinuclear adduct $Ph_3C^+(C_6F_5)_3AlFAl(o\text{-}C_6F_5C_6F_4)_3^-$ (**11**; δ −169.38, $\Delta\delta = +5.64$ ppm) is very large by comparison to the difference between Al−*F* and Al−*F*−Al shifts in **8** and **9** ($\Delta\delta = +1.31$ ppm). The Al−*F* chemical shift in mononuclear **4** is displaced dramatically upfield of that in the mononuclear perfluorophenyl analogue **8**, whereas the Al−*F*−Al resonance of asymmetric $Ph_3C^+(C_6F_5)_3AlFAl(o\text{-}C_6F_5C_6F_4)_3^-$ (**11**) is shifted only slightly upfield of the symmetric dinuclear analogue **9**. Furthermore, the perfluorobiphenyl ^{19}F shifts change drastically upon reaction of $Al(C_6F_5)_3$ with **4** (cf. $\Delta\delta = +5.34$ ppm for the Al-vicinal F atom). Signals for the two *o*-F atoms of the C_6F_5 fragment of the perfluorobiphenyl ligand are magnetically equivalent in **4** but inequivalent in **11**, the same being true of the *m*-F resonances, indicating that rotation about the medial $C_{Ph}-C_{Ph}'$ bond is facile in **4** but is restricted in **11**. The perfluorophenyl ^{19}F NMR signals of **11** are quite similar to those of both **8** and **9**.

The Al-bound perfluorobiphenyl ligands can assume two quite different conformations, according to the crystallographic evidence from **4**[9b] and **11** (Figure 4; selected bond distances and angles are summarized in Table 7): in **4**, the biphenyl ligands are oriented along the Al−F axis and sterically encapsulate the Al-bound F atom, whereas in **11** the biphenyl

(31) See the Supporting Information, giving details of the preparation and characterization of **4**, in ref 9b. Previously unreported ^{19}F NMR chemical shift data for **4** in C_7D_8 at 23 °C are as follows: δ −120.72 (s, 3 F, F-3), −139.52 (s, 3 F, F-6), −141.48 (s, 6 F, F-2′/F-6′), −156.55 (t, 3 F, F-4), −157.22 (s, 3 F, F-4′), −158.46 (t, 3 F, F-5), −165.20 (s, 6 F, F-3′/F-5′), −175.02 (s, br, 1 F, Al−F).

Table 7. Selected Bond Distances and Angles for the Cocatalyst $Ph_3C^+(C_6F_5)_3AlFAl(o\text{-}C_6F_5C_6F_4)_3^-$ (11)

Bond Distances (Å)			
Al1−F1	1.770(3)	Al2−C43	2.010(4)
Al2−F1	1.797(3)	C24−C25	1.485(6)
Al1−C1	1.977(5)	C36−C37	1.489(7)
Al1−C7	1.992(5)	C48−C49	1.486(6)
Al1−C13	1.981(4)	C55−C56	1.430(6)
Al2−C19	2.015(4)	C55−C62	1.435(6)
Al2−C31	1.998(5)	C55−C68	1.453(6)
Bond Angles (deg)			
Al1−F1−Al2	176.91(16)	F1−Al2−C19	100.18(15)
F1−Al1−C1	102.02(16)	F1−Al2−C31	100.60(15)
F1−Al1−C13	105.70(16)	F1−Al2−C43	103.28(15)
F1−Al1−C7	104.32(16)	C56−C55−C68	118.2(4)
C19−C24−C25	123.0(4)	C43−C48−C49	123.9(4)
C1−Al1−C7	113.60(19)	C31−Al2−C19	116.73(18)
C1−Al1−C13	115.87(19)	C43−Al2−C19	116.73(18)
C13−Al1−C7	113.51(18)	C31−Al2−C43	115.21(19)
C56−C55−C62	121.1(4)	C62−C55−C68	120.7(4)
C31−C36−C37	122.2(4)		
Torsion Angles (deg)			
C19−C24−C25−C26		−71.2	
C31−C36−C37−C42		−69.7	
C43−C48−C49−C54		−69.6	

ligands are oriented away from the Al-bound F atom, assuming a mutual stacking arrangement that exposes the Al-bound F atom and imparts a corkscrew motif to the anionic fragment, with each Al-bound C_6F_4 ring lying in close proximity to, and parallel with, the C_6F_5 ring of one adjacent *o*-perfluorobiphenyl ligand. This motif is also seen in the solid-state structure of the ion-pair complex $Me_2C(Cp)(Flu)ZrMe^+FAl(o\text{-}C_6F_5C_6F_4)_3^-$ (obtained from reaction of **4** with **15**), in this case featuring a Zr−F−Al linkage.[12] The observed profound effect of the added $Al(C_6F_5)_3$ unit upon the ^{19}F chemical shift values of both the Al-bound F atom and perfluorophenyl ligands of **4** may derive from a solution-phase rearrangement process that converts the sterically encapsulated, terminal Al−F configuration observed in **4** to the exposed, bridging Al−F−Al configuration observed in **11** (see Table 8 for a detailed comparison of the six anions containing *o*-$C_6F_5C_6F_4$ substituents). The nearly linear Al−F−Al core ($\angle$Al−F−Al = 176.91(16)°) present in the structure of **11** is much like those of previously reported $F[AlMe_3]_2^-$ [32a] and $F[AlEt_3]_2^-$.[32b] However, whereas the alkyl moieties in these latter two anion structures occupy a staggered conformation,[32] the two sets of Al-bound fluoroaryl rings in **11** are substantially eclipsed, as in the case of **10** above, suggesting a pronounced $\pi-\pi$ or steric interaction between the two sets of fluoroaryl rings. The two F−Al bonds in **11** differ slightly in length (F−Al(C_6F_5)$_3$ = 1.770(3) Å and F−Al(*o*-$C_6F_5C_6F_4$)$_3$ = 1.797(3) Å) but are similar to the F−Al bond distances in $F[AlMe_3]_2^-$ (1.783 Å)[32a] while being shorter than in $F[AlEt_3]_2^-$ (1.835 Å), likely due to alkyl−alkyl repulsions in the latter.[32b]

In the reactions of metallocene dimethyl **15** with cocatalysts **8**−**10**, each instance affords $Me_2C(Cp)(Flu)ZrMe^+FAl(C_6F_5)_3^-$ (**18**) together with varying amounts of diastereomeric $[Me_2C(Cp)(Flu)ZrMe]_2(\mu\text{-}Me)^+F[Al(C_6F_5)_3]_2^-$ (**19**; see Scheme 2). These systems do not undergo rapid equilibration: mixtures of **18** and **19** slowly decompose to pure **18**, suggesting either (a) conversion of **19** to **18** together with slow formation and subsequent comparatively rapid decomposition of $Me_2C(Cp)(Flu)ZrMe^+MeAl(C_6F_5)_3^-$ or (b) direct decomposition of **19** to form some insoluble product. Mononuclear **18** is robust with respect to decomposition. Despite the complexity of these reactions, it is found that the catalytically-active species generated via reaction in situ are effective agents for highly syndiospecific propylene polymerization.[17] In the reaction of **15** with $Ph_3C^+FAl(C_6F_5)_3^-$ (**8**), the ion-pair complexes **18** and **19** are initially formed in a ∼1:1 ratio (as assayed from in situ NMR experiments), implying a Zr-mediated Al−F bond cleavage reaction: the mononuclear trityl salt **8** is isolable in pure form, suggesting that the Al−F cleavage process likely involves the reaction of $Me_2C(Cp)(Flu)ZrMe^+FAl(C_6F_5)_3^-$ (**18**) with $FAl(C_6F_5)_3^-$ salt **8** or **18** to generate an ion-pair complex containing the dinuclear $F[Al(C_6F_5)_3]_2^-$ anion, together with unidentified insoluble fluoromethylzirconium species. When metallocene **15** is combined with the cocatalyst $Ph_3C^+F[Al(C_6F_5)_3]_2^-$ (**9**), metallocenium complexes **18** and **19** are initially formed in a 1:2 ratio, demonstrating that the dinuclear $F[Al(C_6F_5)_3]_2^-$ anion can indeed undergo conversion to the mononuclear $FAl(C_6F_5)_3^-$ anion in **18**. The trinuclear cocatalyst $(Ph_3C^+)_2F_2[Al(C_6F_5)_3]_3^-$ (**10**) reacts with **15** to form **18** and **19** in a 2:3 ratio, suggesting that **10** behaves much like a 1:1 mixture of **8** and **9** in the activation of metallocene **15**. In the reaction of **15** with cocatalyst **11** we observe by NMR the exclusive formation of the methyl-bridged species $[Me_2C(Cp)(Flu)ZrMe]_2(\mu\text{-}Me)^+(C_6F_5)_3AlFAl(o\text{-}C_6F_5C_6F_4)_3^-$ (**20**, as diastereomers in a 3:2 ratio) with no detectable mononuclear species (Scheme 2).[33] The Al(*o*-$C_6F_5C_6F_4$)$_3$ moiety, inisolable by itself, confers added stability with no observed formation of complex **18** or $Me_2C(Cp)(Flu)ZrMe^+FAl(o\text{-}C_6F_5C_6F_4)_3^-$.

The Al−*F*−Al ^{19}F chemical shifts in complexes **19** and **20** are much like those of the corresponding cocatalysts, whereas coordination to Zr induces a considerable downfield shift in the Zr−*F*−Al signal of **18** compared with that in cocatalyst **8** (δ −168.61 vs −140.33 ppm). There is an interesting correlation between increasing Al−*F* ^{19}F chemical shift and increasing average Al−F bond distance that obtains regardless of F atom coordination number (1 or 2) or anion nuclearity (1, 2, or 3 Al atoms), across the series **4**, **10**, **11**, **19**, and **20**. This trend does not extend to systems having a Zr−F contact.

The crystal structures of metallocenium complexes **19** and **20** each feature a methyl-bridged dinuclear Zr−Me−Zr cation and an unasssociated, sterically congested F-bridged dinuclear aluminate anion (Figures 5 and 6, respectively). Selected bond distances and angles are summarized in Tables 9 and 10, respectively. The $(C_6F_5)_3AlFAl(o\text{-}C_6F_5C_6F_4)_3^-$ anions in **11** and **20** are metrically similar, with some interesting differences: in

Table 8. Comparison of the Torsion Angles (deg) in $FAl(o\text{-}C_6F_4C_6F_5)_3^-$ and $FB(o\text{-}C_6F_4C_6F_5)_3^-$ Anions

	4[9a]	**4** + **15**[12a]	**7**	**17**	**11**	**20**
anion	$FAl(o\text{-}C_6F_5\text{-}C_6F_4)_3^-$	[Zr]-$FAl(o\text{-}C_6F_5\text{-}C_6F_4)_3^-$	$FB(o\text{-}C_6F_5\text{-}C_6F_4)_3^-$	$FB(o\text{-}C_6F_5\text{-}C_6F_4)_3^-$	[Al]-$FAl(o\text{-}C_6\text{-}F_5C_6F_4)_3^-$	[Al]-$FAl(o\text{-}C_6\text{-}F_5C_6F_4)_3^-$
structure	**J**	**K-2**	**J**	**J**	**K-1**	**K-2**
$C_a-C_b-C_c-C_d$[a]	−53.9	−102.6	−77.9	−59.7	−69.6	−101.8
	−95.3	−102.7	−81.4	−94.4	−69.7	−109.9
	−98.0	−109.2	−94.9	−97.9	−71.2	−118.0
$F-M-C_a-C_b$[a]	−15.0	+119.6	−30.5	−17.9	−119.0	+115.9
	−38.4	+120.1	−32.2	−40.6	−120.6	+119.5
	−38.4	+130.0	−39.2	−42.4	−121.3	+124.8

[a] Torsion angle.

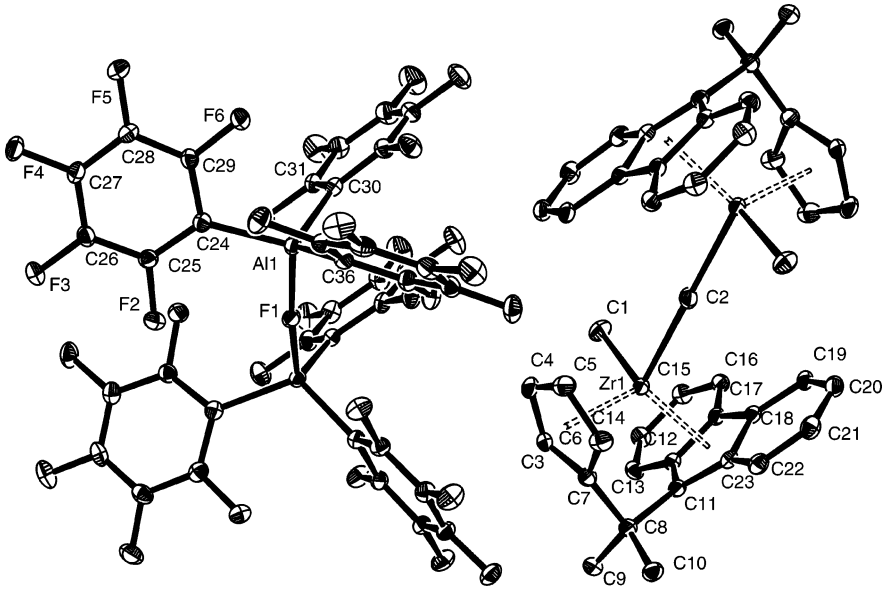

Figure 5. Perspective ORTEP drawing of the molecular structure of the dinuclear Zr−(μ-Me)−Zr complex $[Me_2C(Cp)(Flu)ZrMe]_2(\mu\text{-}Me)^+(C_6F_5)_3AlFAl(C_6F_5)_3^-$ (**19**). Thermal ellipsoids are drawn at the 30% probability level.

Table 9. Selected Bond Distances and Angles for the Dinuclear Metallocene Complex $[Me_2C(Cp)(Flu)ZrMe]_2(\mu\text{-}Me)^+$ $F[Al(C_6F_5)]_3^-$ (19)

Bond Distances (Å)			
Zr1−C2	2.4179(3)	C7−C8	1.530(4)
Al1−F1	1.7945(9)	Al1−C24	1.983(3)
Zr1−Cp_{cent}[a]	2.178	C8−C11	1.553(4)
C1−Zr1	2.248(3)	Al1−C36	1.986(3)
Al1−C30	1.993(3)	Zr1−C8	3.126
Zr1−Flu_{cent}[a]	2.237	Zr1−Zr1′	4.836(6)
Bond Angles (deg)			
Zr1−C2−Zr1′	180	C7−C8−C11	99.5(2)
F1−Al1−C24	105.60(10)	F1−Al1−C36	107.23(11)
C24−Al1−C30	111.32(13)	C36−Al1−C30	112.88(13)
C2−Zr1−C1	92.35(10)	Al1−F1−Al1′	167.10(12)
F1−Al1−C30	104.61(12)	Cp_{cent}−Zr1−Flu_{cent}	118.43
C24−Al1−C36	114.35(13)		

[a] Centroid of C_5 ligand.

Table 10. Selected Bond Distances and Angles for the Dinuclear Metallocene Complex $[Me_2C(Cp)(Flu)ZrMe]_2(\mu\text{-}Me)^+(C_6F_5)_3AlFAl(o\text{-}C_6F_5C_6F_4)_3^-$ (20)

Bond Distances (Å)			
C1B−Zr1	2.443(12)	Al1−C51	1.965(15)
C1B−Zr2	2.393(12)	Al2−C87	2.018(12)
Al1−F1	1.786(7)	Zr2−Cp_{cent}[a]	2.170
Al2−F1	1.785(7)	C15−C18	1.506(14)
Zr1−Cp_{cent}	2.162	C37−C40	1.520(15)
Zr1−Zr2	4.770	Al1−C57	1.945(14)
C1−Zr1	2.278(13)	Al2−C75	2.022(12)
C23−Zr2	2.228(13)	Zr2−Flu_{cent}[a]	2.245
Al1−C45	1.986(12)	Zr1−C15	3.097
Al2−C63	1.992(12)	Zr2−C37	3.105
Zr1−Flu_{cent}	2.251	C68−C69	1.462(16)
Al1−Al2	3.568	C80−C81	1.501(15)
C14−C15	1.566(16)	C91−C92	1.529(17)
C36−C37	1.545(17)		
Bond Angles (deg)			
Zr1−C1B−Zr2	161.1(6)	C18−C15−C14	101.2(9)
Al1−F1−Al2	175.5(4)	C40−C37−C36	101.2(10)
F1−Al1−C45	102.1(4)	F1−Al2−C63	101.2(4)
F1−Al1−C51	102.7(5)	F1−Al2−C75	100.1(4)
F1−Al1−C57	100.3(5)	F1−Al2−C87	99.9(4)
C69−C68−C63	121.9(11)	C87−C91−C92	122.5(11)
C1−Zr1−C1B	91.0(5)	Cp_{cent}−Zr1−Flu_{cent}	119.0
C23−Zr2−C1B	96.3(5)	Cp_{cent}−Zr2−Flu_{cent}	118.1
C51−Al1−C45	115.5(6)	C63−Al2−C87	114.9(5)
C57−Al1−C45	116.4(6)	C63−Al2−C75	117.6(5)
C57−Al1−C51	116.0(6)	C87−Al2−C75	118.0(5)
C75−C80−C81	123.4(10)		

[a] Centroid of C_5 ligand.

11, the bridging F atom is nearer the $Al(C_6F_5)_3$ group (1.770(3) vs 1.797(3) Å), whereas in **20**, it is equidistant from the Al centers (1.786(7) vs 1.785(7) Å). In **11**, **19**, and **20**, the Al coordination tetrahedra are distorted toward $Al(fluoroaryl)_3$ planarity. Interestingly, the $Al(C_6F_5)_3$ moiety of **20** is more planarized than that of **11** (average ∠F−Al−C = 101.7(5) vs 104.01(16)°), and the $(C_6F_5)_3Al$−F bond is correspondingly longer (1.786(7) Å in **20** vs 1.770(3) Å in **11**). We suggest that these differences are largely due to packing forces, and in any case they indicate a certain degree of conformational flexibility about the Al atoms in these structures, with $Al(fluoroaryl)_3$ flattening correlated with a lengthening of the Al−F bond. Similar to the F-bridged polynuclear aluminate cocatalysts **10** and **11**, the sets of Al-bound fluoroaryl rings **19** and **20** are substantially eclipsed.

As in the perfluorobiphenyl groups of cocatalyst **11** and ion-pair complex $Me_2C(Cp)(Flu)ZrMe^+FAl(o\text{-}C_6F_5C_6F_4)_3^-$, the perfluorobiphenyl groups of the anion in complex **20** stack together in a corkscrew structure that exposes the bridging F atom. In contrast, the anionic components of the cocatalyst $Ph_3C^+FB(o\text{-}C_6F_5C_6F_4)_3^-$ (**7**) and ion-pair complex $[Me_2C(Cp)(Flu)ZrMe]_2(\mu\text{-}F)^+FB(o\text{-}C_6F_5C_6F_4)_3^-$ (**17**) feature B-bound F atoms in terminal, encapsulated configurations in both cases and do not exhibit this corkscrew conformational motif. Also, whereas the structure of $Me_2C(Cp)(Flu)ZrMe^+(\mu\text{-}Me)B(C_6F_5)_3^-$ exhibits a B−C−Zr linkage, the previously reported ion-pair complex $[Me_2C(Cp)(Flu)ZrMe]_2(\mu\text{-}Me)^+MeB(o\text{-}C_6F_5C_6F_4)_3^-$ does not,[12] and only the dinuclear Zr−μ-Me−Zr cation is obtained upon reaction of $Me_2C(Cp)(Flu)ZrMe_2$ with $B(o\text{-}C_6F_5C_6F_4)_3$ in toluene-d_8 solution. These data appear to suggest that the cost in degrees of conformational freedom of forming a rigid, corkscrew-packed (perfluorobiphenyl)borate anion outweighs the benefits of

(32) The Al−F−Al bond angle in both complexes is ∼180°. (a) For R = Me: Allegra, G.; Perego, G. *Acta Crystallogr.* **1963**, *16*, 185. (b) For R = Et: Atwood, J. L.; Newberry, W. R., III. *J. Organomet. Chem.* **1974**, *66*, 15.

(33) Pure orange complex **20** can be isolated; however, thermal decomposition in the solid state slowly occurs at room temperature.

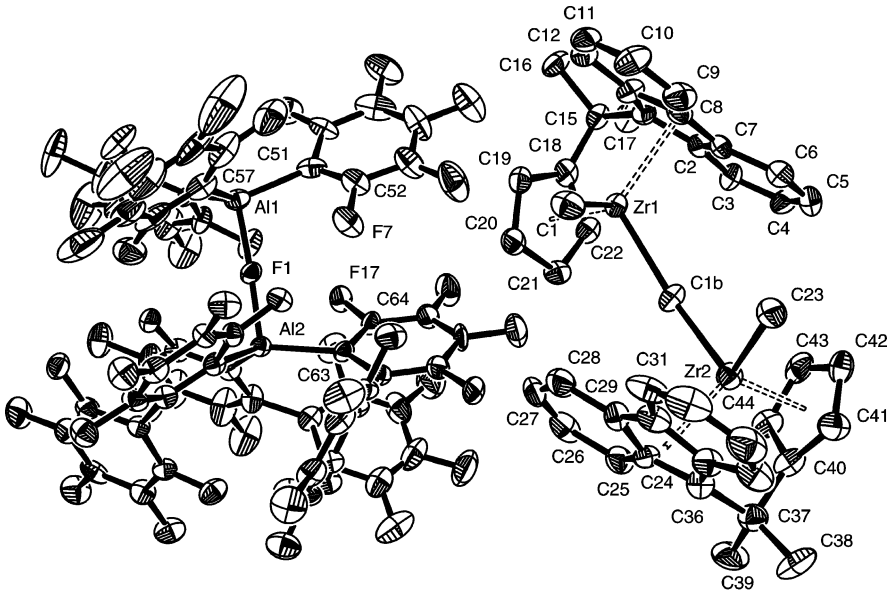

A.

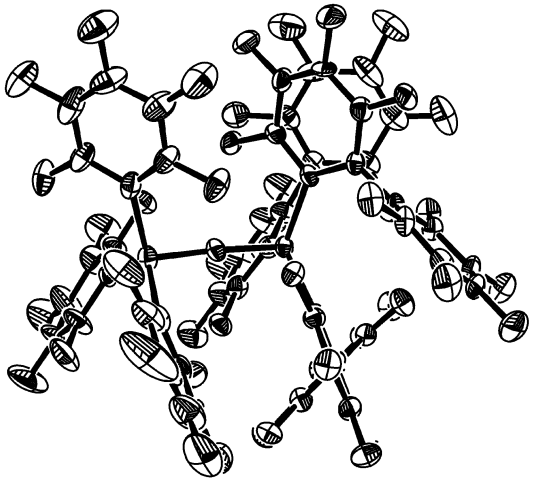

B.

Figure 6. Perspective ORTEP drawings of the molecular structure of (A) the dinuclear Zr−(*μ*-Me)−Zr complex $[Me_2C(Cp)(Flu)ZrMe]_2$-$(\mu\text{-Me})^+(C_6F_5)_3AlFAl(o\text{-}C_6F_5C_6F_4)_3^-$ (**20**) and (B) the anion in **20**. Thermal ellipsoids are drawn at the 30% probability level.

forming a B−C−Zr linkage. It is possible that the B-based systems cannot achieve the corkscrew packing at all, possibly due to the smaller covalent radius of boron and comparative closeness of the C_{aryl}−B contacts. In a comparison of torsion angles among the collected perfluorobiphenyl Al and B anions ($C_a-C_b-C_c-C_d$ or $F-M-C_a-C_b$; see Table 8), it can be seen that the nonbridging, encapsulated forms **G** (see Figure 7) exhibit relatively wide variations in conformation, whereas forms **H** (see Figure 7) are remarkably similar, suggesting that this corkscrew motif is uniquely stable.

The cationic fragments of metallocenium structrures **19** and **20** also exhibit some degree of conformational flexibility: for complex **19**, the methyl-bridged dinuclear cation has a crystallographically enforced linear Zr−Me−Zr configuration (∠Zr1−Me−Zr2 = 180°) and the two zirconocene fragments are essentially identical. For complex **20**, the Me-bridged dinuclear cation has a markedly bent Zr−Me−Zr configuration (∠Zr1−Me−Zr2 = 161.1(6)°) with the two zirconocene fragments having rather different coordination environments (e.g., Zr1−(*μ*-Me) = 2.443(12) Å, Zr2−(*μ*-Me) = 2.393(12) Å, Zr1−$Me_{terminal}$ = 2.278(13) Å, Zr2−$Me_{terminal}$ = 2.228(13) Å; see Table 10). Three other methyl-bridged dinuclear Zr−Me−Zr cation structures, $[(N_3)_2ZrMe)_2(\mu\text{-Me})]^+B(C_6F_5)_4^-$(**I**; N_3 = $MesN(CH_2CH_2)_2NMe$),[34] $\{[(guan)_2ZrMe]_2(\mu\text{-Me})\}^+B(C_6F_5)_4^-$

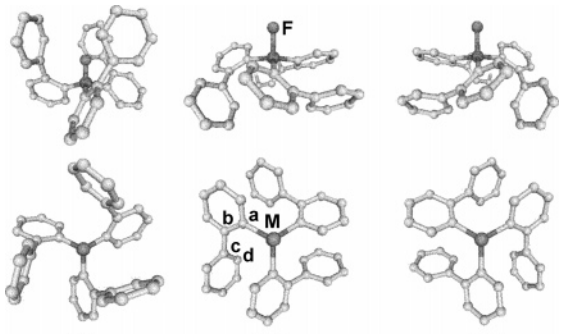

Figure 7. Perspective drawings of free (**G**) and associated (**H**) tris(perfluorobiphenyl)fluorometalate ligands.

(34) Mes = mesityl. See: Schrock, R. R.; Casado, A. L.; Goodman, J. T.; Liang, L.-C.; Bonitatebus, P. J., Jr.; Davis, W. M. *Organometallics* **2000**, *19*, 5325−5341.

Table 11. Comparison of Selected Bond Distances (Å) and Angles (deg) for Dinuclear Metallocene Cations Containing Zr−Me−Zr Linkages

	[Zr]−Me−[Zr]				
	G[34]	**H**[35]	**I**[9a]	**19**	**20**
[Zr]	$(N_3)_2ZrMe$ [h]	$(guan)_2ZrMe$ [i]	$(1,2\text{-}Me_2Cp)ZrMe$	$[Me_2C(Cp)(Flu)]ZrMe$	$[Me_2C(Cp)(Flu)]ZrMe$
anion	$B(C_6F_5)_4^-$	$B(C_6F_5)_4^-$	$MeB(o\text{-}C_6F_5C_6F_4)_3^-$	$(C_6F_5)_3AlFAl(C_6F_5)_3^-$	$(C_6F_5)_3AlFAl(o\text{-}C_6F_5C_6F_4)_3^-$
Zr−(μ-Me)[a]	2.482(25)	2.45(5)	2.424(16)	2.4179(3)	2.418(12)
Zr−Me_t[b]	2.243(13)	2.254(4)	2.242(16)	2.248(3)	2.253(13)
Zr−(μ-Me)−Zr[c]	167.4(4)	170.84(13)	170.9(4)	180	161.1(6)
Me_t−Zr−(μ-Me)[d]	96.0(13)	89.3(8)	93.3(10)	92.35(10)	93.7(5)
Cp_{cent}−Zr−Cp_{cent}[e]			132.41	118.43	118.6
R−Zr−Zr−R[f]	82.0	33.0	108.5	180	−62.8
Zr−Zr[g]	4.933	4.871	4.833	4.836(6)	4.770

[a] Mean bond distance. [b] Mean Zr−Me bond distance. [c] Bond angle. [d] Mean R−Zr−(μ-Me) bond angle. [e] Centroid of C_5 ligand. [f] Torsion angle. [g] Metal distance. [h] $N_3 = (MesNCH_2CH_2)_2NMe$.[34] [i] guan = η^2-(*i*-PrN)$_2$C(NMe$_2$).[35]

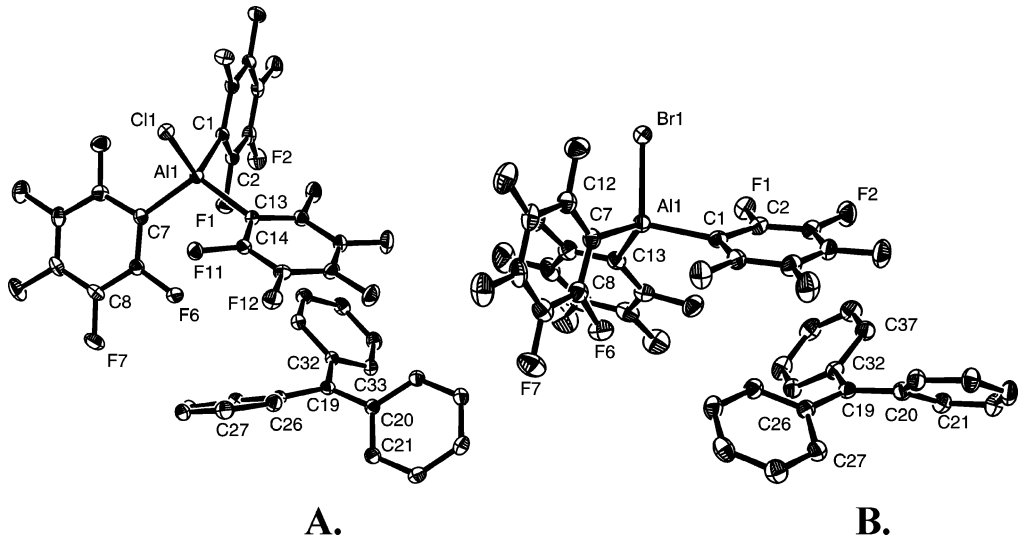

Figure 8. Perspective ORTEP drawings of the molecular structures of the cocatalyst reagents (A) $Ph_3C^+ClAl(C_6F_5)_3^-$ (**12**) and (B) $Ph_3C^+BrAl(C_6F_5)_3^-$ (**13**). Thermal ellipsoids are drawn at the 30% probability level.

(**J**),[35] and $[(Cp''_2ZrMe)_2(\mu\text{-}Me)]^+$ $MeB(o\text{-}C_6F_4C_6F_5)_3^-$ (**K**),[9a] have been reported, and relevant bond distances and angles are presented in Table 11.

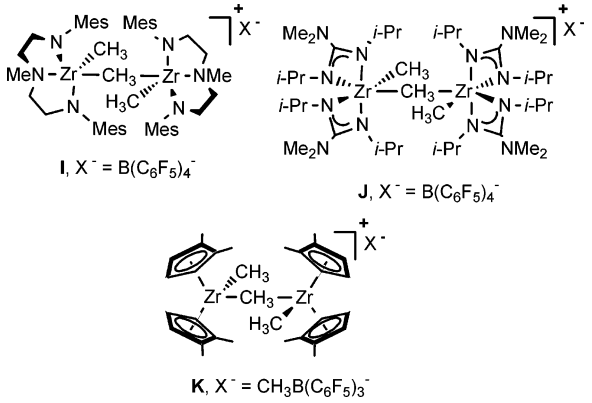

B. Trityl Perfluoroaryl Haloaluminates $Ph_3C^+XAl(C_6F_5)_3^-$ (X = Cl, 12; X = Br, 13). The reaction of trityl chloride or trityl bromide with **3** in a 1:1 ratio yields trityl tris(perfluorophenyl)chloro- and tris(perfluorophenyl)bromoaluminates ($Ph_3C^+XAl(C_6F_5)_3^-$: X = Cl, 78% yield, **12**; X = Br, yield **13**; eq 9), evidenced by the appearance of three new fluoroaryl resonances in the ^{19}F NMR spectra of these reaction mixtures. Both complexes were further characterized by X-ray diffractometry (Figure 8) and are, to the authors' knowledge, the first reported triarylchloro-[36] and triarylbromoaluminate[37] complexes. Selected bond distances and angles are summarized in Table 12. Both structures feature a noncoordinating trityl cation and pseudotetrahedral (perfluoroaryl)metalate anion. The Al−Cl bond distance in **12** (2.1676(7) Å) is shorter than that in PPN^+-$ClAl(t\text{-}Bu)_3^-$ (2.251(3) Å).[36a] Similarly, the present Al−Br distance (2.332(2) Å) is considerably shorter than in the first reported $BrAlR_3^-$ anion (2.439(3) Å, R = 1-adamantyl, $C_{10}H_{15}$).[37]

In the reaction of metallocene **15** with chloroaluminate **12** or bromoaluminate **13**, formation of a mononuclear ion pair is expected ($M^+ClAlR_3^-$ [38] and $M^+BrAlR_3^-$ [39] species are well-known). However, in each of these three reactions, rapid methide abstraction is observed by in situ NMR along with the

(35) Guan = η^2-(^{i}PrN)$_2$C(NMe$_2$). See: Duncan, A. P.; Mullins, S. M.; Arnold, J.; Bergman, R. G. *Organometallics* **2001**, *20*, 1808−1819.

(36) The structure of $PPN^+ClAlR_3^-$ has been characterized (PPN = bis(triphenylphosphine)nitrogen). See the following, for example. (a) R = *tert*-butyl, see: Harlan, C. J.; Bott. S. G.; Barron, A. R. *J. Am. Chem. Soc.* **1995**, *117*, 6465−6474. (b) R = *tert*-amyl (CMe_2Et), see: Harlan, C. J.; Gillan, E. G.; Bott, S. G.; Barron, A. R. *Organometallics* **1996**, *15*, 5479−5488. (c) The structure of the chloro-bridged dinuclear aluminate $K^+Cl[AlMe_3]_2^-$ has also been characterized crystallographically; see: Atwood, J. L.; Rodgers, R. D.; Hrncir, D. C.; Zaworotko, M. J.; Hunter, W. E. *Acta Crystallogr., Sect. A: Cryst. Phys., Diffr., Theor. Crystallogr.* **1981**, *C83*. (d) The structure of the chloroalane $(\mu_2\text{-}Cl)_2[Al(C_6F_5)_2]_2$, generated via reaction of $Al(C_6F_5)_3$ with CH_2Cl_2, has also been reported; see: Chakraborty, D.; Chen, E. Y.-X. *Inorg. Chem. Commun.* **2002**, *9*, 698−701.

(37) $Mg_3BrCl_3(OEt)(Et_2O)_6^+$ is the countercation; see: Vohs, J. K.; Downs, L. E.; Barfield, M. E.; Latibeaudiere, K. L.; Robinson, G. H. *J. Organomet. Chem.* **2003**, *666*, 7−13.

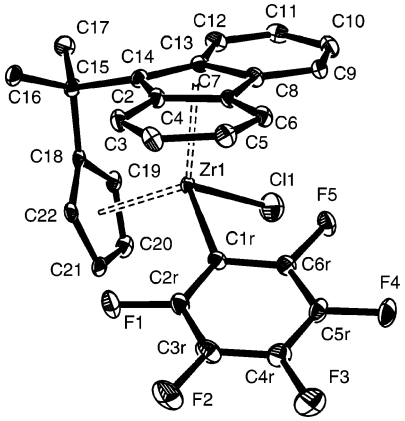

Figure 9. Perspective ORTEP drawing of the molecular structure of $Me_2C(Cp)(Flu)ZrCl(C_6F_5)$ (**21**). Thermal ellipsoids are drawn at the 50% probability level.

Table 12. Selected Bond Distances and Angles for the Cocatalysts $Ph_3C^+ClAl(C_6F_5)_3^-$ (12) and $Ph_3C^+BrAl(C_6F_5)_3^-$ (13)

12		**13**	
	Bond Distances (Å)		
Cl1−Al1	2.1676(7)	Br1−Al1	2.3317(18)
Al1−C1	2.0043(19)	Al1−C1	2.019(4)
Al1−C7	2.0046(19)	Al1−C7	1.998(4)
Al1−C13	2.0143(19)	Al1−C13	2.001(5)
C19−C20	1.441(3)	C19−C20	1.448(5)
C19−C26	1.445(2)	C19−C26	1.435(5)
C19−C32	1.451(2)	C19−C32	1.436(6)
	Bond Angles (deg)		
Cl1−Al1−C1	112.88(6)	Br1−Al1−C1	103.98(11)
Cl1−Al1−C7	105.68(6)	Br1−Al1−C7	112.69(12)
Cl1−Al1−C13	104.56(6)	Br1−Al1−C13	104.90(13)
C1−Al1−C7	108.88(8)	C1−Al1−C7	111.71(18)
C1−Al1−C13	111.26(8)	C1−Al1−C13	114.37(17)
C7−Al1−C13	113.47(8)	C7−Al1−C13	109.00(17)
C20−C19−C26	119.50(16)	C20−C19−C26	119.3(4)
C20−C19−C32	119.68(16)	C20−C19−C32	119.9(4)
C26−C19−C32	120.81(16)	C26−C19−C32	120.8(3)

formation of complex mixtures, precluding further unambiguous characterization of the products. Attempts to isolate individual species as single crystals from these mixtures yielded the decomposition products $Me_2C(Cp)(Flu)ZrCl(C_6F_5)$ (**21**; Figure 9; from **15** + **12**) and $[Me_2C(Cp)(Flu)Zr(\mu_2\text{-}Br)]_2^{2+}[Al(C_6F_5)_4^-]_2$ (**22**; Figure 10; from **15** + **13**), which were characterized by X-ray diffractometry. Selected bond distances and angles are summarized in Tables 13 (for **21**) and 14 (for **22**). Formation of these decomposition products suggests that the Br−Al and Cl−Al interactions are considerably less robust than the analogous Al−F linkages.

V. The Trityl (Perfluoroaryl)fluorogallate $Ph_3C^+F[Ga(C_6F_5)_3]_2^-$ (14). Trityl fluorobis[tris(perfluorophenyl)gallate] ($Ph_3CF^+[Ga(C_6F_5)_3]_2^-$; **14**) is derived from a "one-pot" reaction of trityl fluoride with $Ga(C_6F_5)_3$ (**5**), in turn generated in situ via alkyl−aryl metathesis of $B(C_6F_5)_3$ with $Ga(CH_3)_3$ (eq 8).[40]

Table 13. Selected Bond Distances and Angles for $Me_2C(Cp)(Flu)ZrCl(C_6F_5)$ (21)

	Bond Distances (Å)		
Cl1−Zr1	2.4225(19)	Zr1−C15	3.1137
C2R−C3R	1.382(8)	C15−C18	1.533(8)
Zr1−Cp_{cent}[a]	2.178	C5R−C6R	1.362(8)
C1R−Zr1	2.351(5)	C2R−F1	1.364(6)
C3R−C4R	1.373(9)	C1R−C2R	1.380(7)
Zr1−Flu_{cent}[a]	2.239	C1R−C6R	1.394(7)
C14−C15	1.556(7)	C6R−F5	1.357(6)
C4R−C5R	1.386(9)		
	Bond Angles (deg)		
C1R−Zr1−Cl1	99.44(14)	Cp_{cent}−Zr1−Flu_{cent}	118.2
C6R−C1R−Zr1	113.8(4)	C2R−C1R−C6R	113.2(5)
C18−C15−C14	98.7(4)	C2R−C1R−Zr1	133.0(4)
	Torsion Angles (deg)		
Cl−Zr−C1R−C6R		39.4	
Cl−Zr−C1R−C2R		−138.7	

[a] Centroid of C_5 ligand.

Table 14. Selected Bond Distances and Angles for $[Me_2C(Cp)(Flu)Zr(\mu_2\text{-}Br)]_2^{2+}[Al(C_6F_5)_4^-]_2$ (22)

	Bond Distances (Å)		
Br1−Zr1	2.6772(13)	C13−C14	1.459(12)
Al1−C23	2.027(10)	Al1−C35	2.019(10)
Zr1−Cp_{cent}[a]	2.135	Zr1−Zr2	3.896
Br1′-Zr1	2.7155(13)	C15−C18	1.537(13)
Al1−C29	2.023(10)	Al1−C41	2.023(10)
Zr1−Flu_{cent}[a]	2.197	Zr1−C14	3.093
	Bond Angles (deg)		
Zr1−Br1−Zr1′	92.52(4)	C41−Al1−C35	111.5(4)
C35−Al1−C23	105.6(4)	C23−Al1−C29	109.2(4)
C41−Al1−C29	105.7(4)	C35−Al1−C29	111.9(4)
Br1−Zr1−Br1′	87.48(4)	Cp_{cent}−Zr1−Flu_{cent}	120.2

[a] Centroid of C_5 ligand.

Several products are observed in this reaction; however, pure **14** can be isolated in good yield (67%) by fractional crystallization. In addition to three fluoroaryl ^{19}F signals, the ^{19}F NMR spectrum of **14** exhibits a characteristic broad upfield resonance at δ −210.11 ppm, indicative of Ga−F bond formation. Furthermore, the 12:6:12:1 integral ratio of these resonances reveals that one F atom is bound to two Ga moieties. The structure of **14** was confirmed by X-ray diffraction as the first linear fluoro-bridged organogallium complex,[41] as shown in Figure 11. Selected bond distances and angles are summarized in Table 15. Similar to the case for **10**, the two Ga centers are connected by one F atom with a nearly linear Ga−F−Ga configuration (173.37(12)°). This bridged Ga−F bond distance (1.907(11) Å, average) is longer (0.069 Å) then the terminal Ga−F bond distances in both $GaF(Bz)_2(Bu^tNH_2)$[41c] and $GaF(Mes)_2(Bu^tNH_2)$ [41d] (1.828 and 1.838 Å, respectively). The six fluoroaryl rings attached to the two Ga centers are substantially eclipsed as in **11**, again reflecting possible $\pi-\pi$ stacking or steric interactions between sets of fluoroaryl rings.

In the reaction of metallocene **15** with the dinuclear, fluoro-bridged dinuclear gallate **14**, a pair of diastereomeric μ-methyl complexes similar to **19** or **20** would be expected, a priori. However, in this reaction as well, rapid methide abstraction is

(38) For [Ti]−$ClAlMe_3$, see: (a) Coles, M. P.; Hitchcock, P. B. *Dalton Trans.* **2001**, *8*, 1169−1171. (b) Kelly, D. G.; Toner, A. J.; Walker, N. M.; Coles, S. J.; Hursthouse, M. B. *Polyhedron* **1996**, *15*, 4307−4310. For [Zr]−$ClAl(t\text{-}Bu)_3$, see: (c) Reference 36a. For [Ta]−$ClAlMe_3$, see: (d) Churchill, M. R.; Wasserman, H. J.; Turner, H. W.; Schrock, R. R. *J. Am. Chem. Soc.* **1982**, *104*, 1710−1716. For $([Cr]-Me-[Cr])^+ClAlMe_3^-$, see: (e) Wei, P.; Stephan, D. W. *Organometallics* **2003**, *22*, 1712−1717. For [Cr]−$ClAlMe_3$, see: (f) Sugiyama, H.; Aharonian, G.; Gambarotta, S.; Yap, G. P. A.; Budzelaar, P. H. M. *J. Am. Chem. Soc.* **2002**, *124*, 12268−12274.

(39) For the only characterized structure, [Ti]−$BrAlMe_3$, see: Coles, S. J.; Hursthouse, M. B.; Kelly, D. G.; Walker, N. M. *J. Organomet. Chem.* **1999**, *580*, 304.

(40) (a) Klosin, J.; Roof, G. R.; Chen, E. Y.-X.; Abboud, K. A. *Organometallics* **2000**, *19*, 4684. (b) Hair, G. S.; Cowley, A. H.; Gorden, J. D.; Jones, J. N.; Jones, R. A.; Macdonald, C. L. B. *Chem. Commun.* **2003**, *3*, 424−425.

(41) For recent examples of organogallium−F complexes, see: (a) Werner, B.; Kräuter, T.; Neumüller, B. *Organometallics* **1996**, *15*, 3746−3751. (b) See ref 30a for examples of nonlinear fluoro-bridged Ga complexes. (c) Kopp, M. R.; Neumuller, B. *Z. Anorg. Allg. Chem.* **1999**, *625*, 1413. (d) Kräuter, T.; Neumuller, B. *Z. Anorg. Allg. Chem.* **1995**, *621*, 597−606.

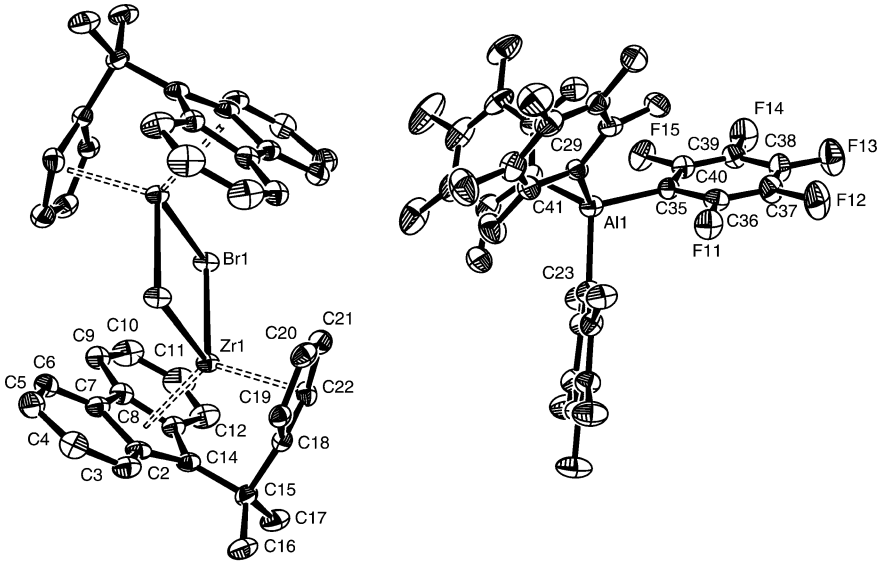

A. **B.**

Figure 10. Perspective ORTEP drawings of the molecular structure of (A) the $[Me_2C(Cp)(Flu)Zr(\mu_2\text{-}Br)]_2^{2+}$ dication in the complex $[Me_2C(Cp)(Flu)Zr(\mu_2{-}Br)]_2^{2+}[Al(C_6F_5)_4^-]_2$ (**22**) and (B) the $Al(C_6F_5)_4^-$ monoanion. Thermal ellipsoids are drawn at the 30% probability level.

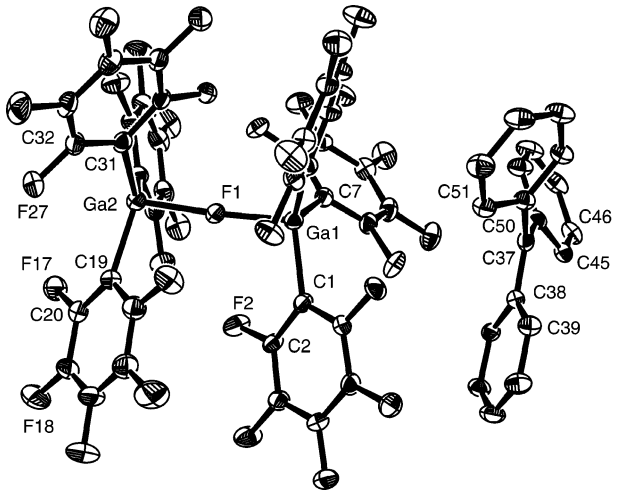

Figure 11. Perspective ORTEP drawing of the molecular structure of the cocatalyst reagent $Ph_3C^+F[Ga(C_6F_5)_3]_2^-$ (**14**). Thermal ellipsoids are drawn at the 30% probability level.

Table 15. Selected Bond Distances and Angles for the Cocatalyst $Ph_3C^+F[Ga(C_6F_5)_3]_2^-$ (14)

Bond Distances (Å)			
F1−Ga1	1.896(2)	C19−Ga2	1.992(4)
F1−Ga2	1.918(2)	C25−Ga2	1.988(4)
C1−Ga1	1.991(4)	C31−Ga2	1.989(4)
C7−Ga1	1.994(4)	C37−C38	1.436(5)
C13−Ga1	2.003(4)	C37−C44	1.444(6)
Bond Angles (deg)			
F1−Ga1−C1	103.02(13)	F1−Ga2−C31	100.08(12)
F1−Ga1−C7	101.02(13)	C19−Ga2−C25	119.52(16)
F1−Ga1−C13	102.78(13)	C19−Ga2−C31	116.77(16)
C1−Ga1−C7	113.98(16)	C25−Ga2−C31	117.25(16)
C1−Ga1−C13	116.23(16)	C38−C37−C44	122.2(3)
C7−Ga1−C13	116.61(16)	C38−C37−C50	119.7(4)
F1−Ga2−C19	97.39(13)	C44−C37−C50	118.1(3)
F1−Ga2−C25	98.11(13)		

observed by NMR along with the formation of multiple unidentifiable, unisolable species.

Conclusions

The evolution of metallocene-catalyzed olefin polymerization chemistry has led to development of a wide array of group 4 metallocene dihalides and dialkyls. Structure−function relationships based on differences among these metallocenes are generally well-understood, aided in part by the development of molecular activators allowing correlations between active catalyst system structural and electronic properties and polymerization performance. Recent advances in understanding the relationship between ion-pairing dynamics and polymerization properties has underscored the significance of the cocatalyst/activator and the resulting anionic fragment in determining polymerization activity and active catalyst thermal stability, as well as product polymer molecular weight and microstructure. The possibility that cocatalyst research can lead to improvements not only in catalyst system performance but also in our mechanistic understanding of polymerization processes provides impetus for the directed expansion of the library of viable activator species.

With findings on the synthesis, chemical properties, and remarkable polymerization behavior of first-generation (perfluoroaryl)fluoroaluminate cocatalyst **7** as a starting point, a broad new family of mono- and polynuclear trityl salts featuring one or more group 13−halide linkages has been developed[16] and is expanded and discussed in the present contribution, with detailed syntheses and characterization and with X-ray crystallographic analysis in most cases. Beyond the development of new cocatalyst species, this work constitutes a complete survey of the chemical behavior of species **1**−**5** as synthons, leading to a general understanding of the interaction between trityl halides and very strong Lewis acid (perfluoroaryl)metalloid species of the class represented by $B(C_6F_5)_3$. Trityl salts **6**−**14** constitute a new class of synthetically accessible cocatalysts for single-site olefin polymerization. Their behavior as activators for the archetypal C_s-symmetric zirconocene dialkyl **15** has been explored in detail and demonstrates efficient and rapid activation by these new cocatalysts, again with structural analysis of products in most cases. In a companion report,[17] we present a detailed mechanistic study of polymerization behavior with these

new cocatalysts with respect to both the C_s-symmetric precatalyst **15** and C_1-symmetric precatalyst Me_2Si(CpR*)(octahydrofluorenyl)$ZrMe_2$ (R* = (1*R*,2*S*,5*R*)-*trans*-5-methyl-*cis*-2-(2-propyl)cyclohexyl; (−)-menthyl). In certain noteworthy cases, we observe enhancements *both* in stereoselectivity *and* in polymerization activity, in contrast to the selectivity−reactivity pattern that has generally been observed thus far in catalytic metallocene olefin polymerization systems.[1,2] These findings represent a significant advancement in overall catalyst system performance derived from cocatalyst development.

Acknowledgment. Financial support by the DOE (Contract No. DE-FG02-86ER1351) is gratefully acknowledged. M.-C.C. thanks Dow Chemical for a postdoctoral fellowship, Dr. M. Oishi for helpful discussions, and Dr. P. Nickias of Dow for GPC measurements. C.Z. thanks the Italian CNR for a postdoctoral fellowship, and A.M.S. thanks the University of Jordan for a sabbatical leave.

Supporting Information Available: CIF files giving complete X-ray experimental details and tables of bond lengths, angles, and positional parameters for the 11 crystal structures in this paper. This material is available free of charge via the Internet at http://pubs.acs.org.

OM0508334